AD-A195 179 ION GUN GENERATED ELECTROMAGNETIC INTERFERENCE ON THE SCATHA SATELLITE(U) NAVAL POSTGRADUATE SCHOOL MONTEREY CA L E WEDDLE DEC 87 1/1

UNCLASSIFIED F/G 22/2 NL

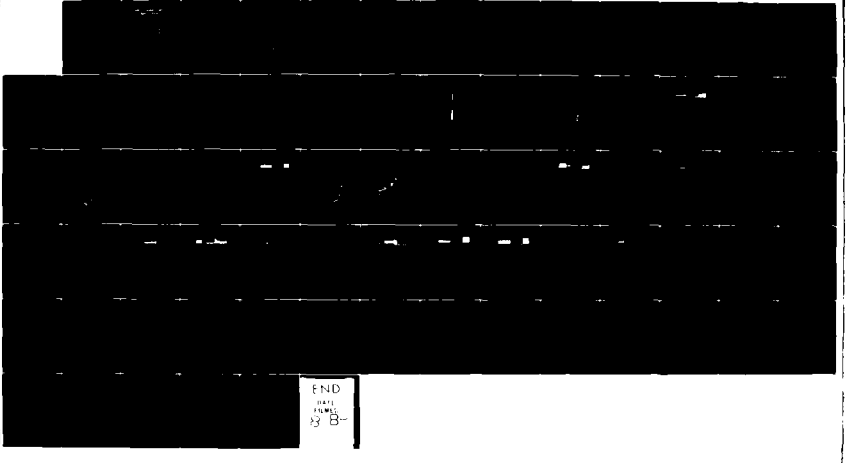

END
DATE FILMED
3 8-

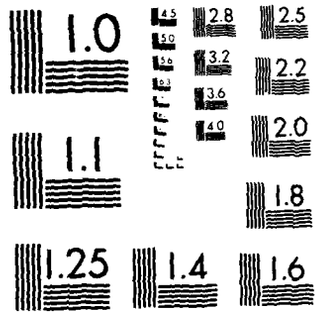

NAVAL POSTGRADUATE SCHOOL
Monterey, California

THESIS

ION GUN GENERATED ELECTROMAGNETIC INTERFERENCE ON THE SCATHA SATELLITE

by

Leonard Earl Weddle

December 1987

Thesis Advisor: R. C. Olsen

SECURITY CLASSIFICATION OF THIS PAGE

REPORT DOCUMENTATION PAGE

1a REPORT SECURITY CLASSIFICATION UNCLASSIFIED	1b RESTRICTIVE MARKINGS NONE
2a SECURITY CLASSIFICATION AUTHORITY NA	3 DISTRIBUTION/AVAILABILITY OF REPORT Approved for public release; distribution is unlimited.
2b DECLASSIFICATION/DOWNGRADING SCHEDULE NA	
4 PERFORMING ORGANIZATION REPORT NUMBER(S)	5 MONITORING ORGANIZATION REPORT NUMBER(S)
6a NAME OF PERFORMING ORGANIZATION Naval Postgraduate School 6b OFFICE SYMBOL (If applicable) 33	7a NAME OF MONITORING ORGANIZATION Naval Postgraduate School
6c ADDRESS (City, State, and ZIP Code) Monterey, California 93943-5100	7b ADDRESS (City, State, and ZIP Code) Monterey, California 93943-5100
8a NAME OF FUNDING/SPONSORING ORGANIZATION 8b OFFICE SYMBOL (If applicable)	9 PROCUREMENT INSTRUMENT IDENTIFICATION NUMBER
8c ADDRESS (City, State, and ZIP Code)	10 SOURCE OF FUNDING NUMBERS PROGRAM ELEMENT NO / PROJECT NO / TASK NO / WORK UNIT ACCESSION NO

11 TITLE (Include Security Classification)
ION GUN GENERATED ELECTROMAGNETIC INTERFERENCE ON THE SCATHA SATELLITE.

12 PERSONAL AUTHOR(S)
Weddle, Leonard E.

13a TYPE OF REPORT Master's Thesis	13b TIME COVERED FROM _____ TO _____	14 DATE OF REPORT (Year, Month, Day) 1987 December	15 PAGE COUNT 73

16 SUPPLEMENTARY NOTATION

17 COSATI CODES			18 SUBJECT TERMS (Continue on reverse if necessary and identify by block number)
FIELD	GROUP	SUB-GROUP	Ion gun, Ion beam, Plasma waves, ~~SCATHA~~, Spacecraft charge control, Satellite charging, Artificial particle beams

19 ABSTRACT (Continue on reverse if necessary and identify by block number)

Spacecraft charging at geosynchronous orbit can cause satellite anomalies and failure. Experiments in charge control were conducted on the joint Air Force/NASA P78-2 (SCATHA) satellite using both electron and positive ion emission systems. These experiments were monitored by a variety of plasma wave and particle detectors. Plasma wave data show that arcing was taking place during non-neutralized ion beam emission. The arcing was seen to cease when either the beam was neutralized or the beam acceleration voltage was turned off. Evidence exists which indicate that the arcing is due to differential charging on the satellite surface. A possible effect of non-neutral, non-accelerated ion beam emission is the shielding of the electric field antenna from ion gun generated plasma waves. The effect of shielding these signals is an increase in the sensitivity of the electric field receiver to natural signals.

20 DISTRIBUTION/AVAILABILITY OF ABSTRACT ☒ UNCLASSIFIED/UNLIMITED ☐ SAME AS RPT ☐ DTIC USERS	21 ABSTRACT SECURITY CLASSIFICATION UNCLASSIFIED
22a NAME OF RESPONSIBLE INDIVIDUAL Olsen, Richard C.	22b TELEPHONE (Include Area Code) 408-646-2019 22c OFFICE SYMBOL 61OS

DD FORM 1473, 84 MAR 83 APR edition may be used until exhausted
All other editions are obsolete

SECURITY CLASSIFICATION OF THIS PAGE

☆ U.S. Government Printing Office: 1986—606-24

UNCLASSIFIED

Approved for public release; distribution is unlimited.

Ion Gun Generated Electromagnetic Interference on the SCATHA Satellite

by

Leonard Earl Weddle
Lieutenant, United States Navy
B.S., Purdue University, 1979

Submitted in partial fulfillment of the requirements for the degree of

MASTER OF SCIENCE IN PHYSICS

from the

NAVAL POSTGRADUATE SCHOOL
December 1987

Author: Leonard Earl Weddle
Leonard Earl Weddle

Approved by: Richard Christopher Olsen
Richard C. Olsen, Thesis Advisor

S. Gnanalingam, Second Reader

K. E. Woehler, Chairman, Department of Physics

Gordon E. Schacher, Dean of Science and Engineering

ABSTRACT

Spacecraft charging at geosynchronous orbit can cause satellite anomalies and failure. Experiments in charge control were conducted on the joint Air Force/NASA P78-2 (SCATHA) satellite using both electron and positive ion emission systems. These experiments were monitored by a variety of plasma wave and particle detectors. Plasma wave data show that arcing was taking place during non-neutralized ion beam emission. The arcing was seen to cease when either the beam was neutralized or the beam acceleration voltage was turned off. Evidence exists which indicate that the arcing is due to differential charging on the satellite surface. A possible effect of non-neutral, non-accelerated ion beam emission is the shielding of the electric field antenna from ion gun generated plasma waves. The effect of shielding these signals is an increase in the sensitivity of the electric field receiver to natural signals.

TABLE OF CONTENTS

LIST OF FIGURES

PAGE

I. INTRODUCTION

A. PROBLEM OF SATELLITE CHARGING

A probe immersed in a plasma will reach an equilibrium potential where the sum of the charging currents to the probe is zero. A rocket or satellite in the ionosphere or magnetosphere is just such a probe. The largest currents in the space environment are due to incident ambient electrons and ions, photoemission, and secondary emission. Experimental results show that satellites typically charge to potentials comparable to the thermal energy of the ambient plasma, in eclipse. In sunlight, positive potentials of a few volts are found due to the dominance of photoemission at high altitudes. Satellite charging is generally not a problem at low altitudes because of low plasma temperatures and high densities. Satellites at high altitudes, such as those in geosynchronous orbits, however, can experience charging into the negative kilovolt range. Clearly a satellite carrying experiments designed to study the satellite environment will have problems doing so if the satellite is always changing its potential relative to the surrounding plasma. Of much greater concern to most satellite users though is electrical discharges caused by differential charging. A satellite's surface is made of many different materials, some of which are conductors and

some dielectrics. These different materials can charge to greatly different potentials. When the potential difference between two surfaces is of sufficient magnitude, an electrical discharge will occur. The current thus induced can cause anomalous commands to be sent to satellite systems, minor or major damage to satellite components, and sometimes complete system or satellite failure. (Refs. 1,2,3,4)

B. HISTORY OF ACTIVE EXPERIMENTS

The P78-2 (SCATHA) satellite was created to study satellite charging and provided with active charge control devices, e.g. ion and electron guns. The SCATHA satellite was the first satellite at geosynchronous orbit capable of observing VLF plasma waves during operation of a positive ion emission system. There have been, however, many experiments conducted in the ionosphere with ion beams carried aloft by rockets that also carried plasma wave receivers.

The Porcupine sounding rocket carried a Xe^+ ion gun. During ion gun experiments electrostatic emissions were detected at harmonics of H^+ and O^+ cyclotron frequencies and near the lower hybrid frequency (Refs. 5,6,7,8). The ARCS rockets carried Ar^+ ion guns. These experiments observed many low frequency electrostatic emissions with the most abundant being near the lower hybrid frequency and some

also near the upper hybrid frequency (Refs. 9,10).

Two Ar^+ ion generators were flown on a sounding rocket launched from Sondre Stromfjord, Greenland to study ion beam dynamics and ion beam effects on the ionosphere. The generators were arranged such that one emitted its beam parallel to the magnetic field and the other one perpendicular. During parallel beam operations emissions were observed near multiples of the H^+ cyclotron frequency and the lower hybrid frequency. Perpendicular beam operations produced emissions at He^+ and O^+ cyclotron harmonics (Ref. 11).

C. THEORETICAL EXPECTATIONS

A limited number of theoretical calculations have been done for such ion beam experiments. They predict the hydrogen cyclotron harmonics and the upper and lower hybrid frequencies observed (Refs. 5,7,9,10,12,13). These experiments took place in the ionosphere where H^+ is a minor constituent. At geosynchronous orbit the environment is mostly H^+ with O^+ ranging from 10 to 50 percent and the beam density large compared to the ambient. The magnetic field strength is also different in the two regions. While these differences prevent us from applying the results of these calculations to our situation, they do give us ideas on where to start looking. We believe it is reasonable to assume that plasma waves at some frequency

would be generated by the SCATHA ion gun. At the SCATHA orbital altitudes, the H^+ cyclotron frequency and the lower hybrid frequency are too low to be observed by the SC1 experiment, although a second receiver (SC1Ø) is occasionally available for this lower frequency regime. The electron cyclotron frequency was generally a few kilohertz. The majority of the work which follows deals with this higher frequency range.

II. SCATHA PROGRAM

A. SATELLITE

The P78-2 satellite was launched January 30, 1979 as part of a joint Air Force/NASA program to study Spacecraft Charging AT High Altitude (SCATHA). It was placed into a nearly geosynchronous orbit with a 7.9 degree inclination, 5.3 R_E perigee, and 7.8 R_E apogee. The cylindrically shaped satellite measures 1.7 meters in diameter and 1.75 meters high. Its surface is made up of insulating and conducting surfaces. The sides are covered primarily by insulating solar cell glass covers. The forward end of the satellite is a conducting surface while the after end is mostly composed of insulators. The satellite was spin stabilized with a period of about 60 seconds with its spin axis in the plane of the orbit and nearly perpendicular to the earth - sun line. The Appendix has a list of the experiments carried on SCATHA and Figure 1 shows the positions of some of the experiments on the satellite. The P78-2 experiments used for this work are the ion gun and plasma wave experiments. (Refs. 14,15,16)

B. ION GUN EXPERIMENT

The ion gun experiment (SC4 - 2) was designed to emit positive charge, to induce negative voltages, and to test

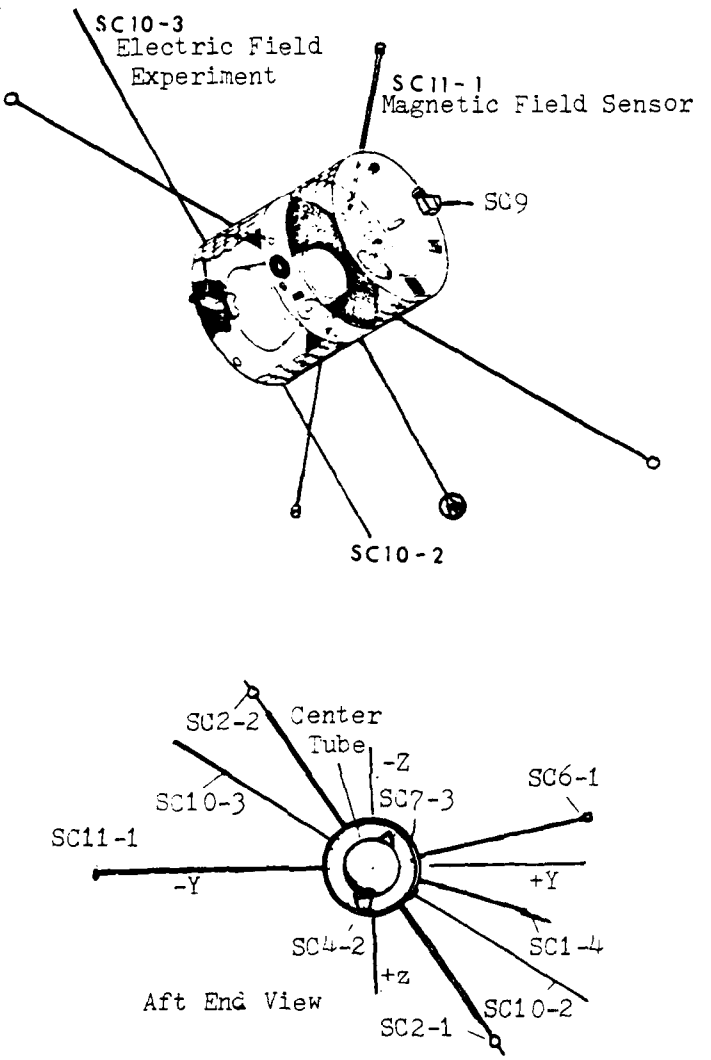

Figure 1. The P78-2 SCATHA satellite.

the effectiveness of ion beams in controlling charging. The experiment included a positive ion emission system and an electron source which could be used to neutralize the beam of ions or to provide electrons alone. The ion system used a cathode discharge to ionize xenon gas which could then be accelerated by either a 1 kV or 2 kV potential between the cathode and exit aperture. The ion current could be varied in increments from Ø.3 mA to 2 mA. Figure 2 is a block diagram of the ion gun and Figure 3 is an electrical schematic. The Appendix lists ion gun commands and functions. (Ref. 17)

C. DETECTORS

The primary diagnostic used in this work is the plasma wave receiver. A portion of the SC1 experiment was a VLF wave experiment. The experiment used the SC1Ø dipole antenna for electric field measurements and an air - core loop for magnetic field measurements. The dipole antenna measures 1ØØ m tip - to - tip. The two halves extend perpendicular to the spin axis. The inner 3Ø m of each half is coated with Kapton insulation. The loop antenna is electrostatically shielded and mounted on a 2 m boom. Its effective area is 575 m^2 at 1.3 kHz. The electric field receiver has sensitivities of 5 x $1Ø^{-7}$ and $1Ø^{-7}$ $V/(mHz^{1/2})$ at 1.3 and 1Ø.5 kHz respectively. The magnetic field receiver has a sensitivity of 3 x $1Ø^{-6}$ $nT/Hz^{1/2}$ at

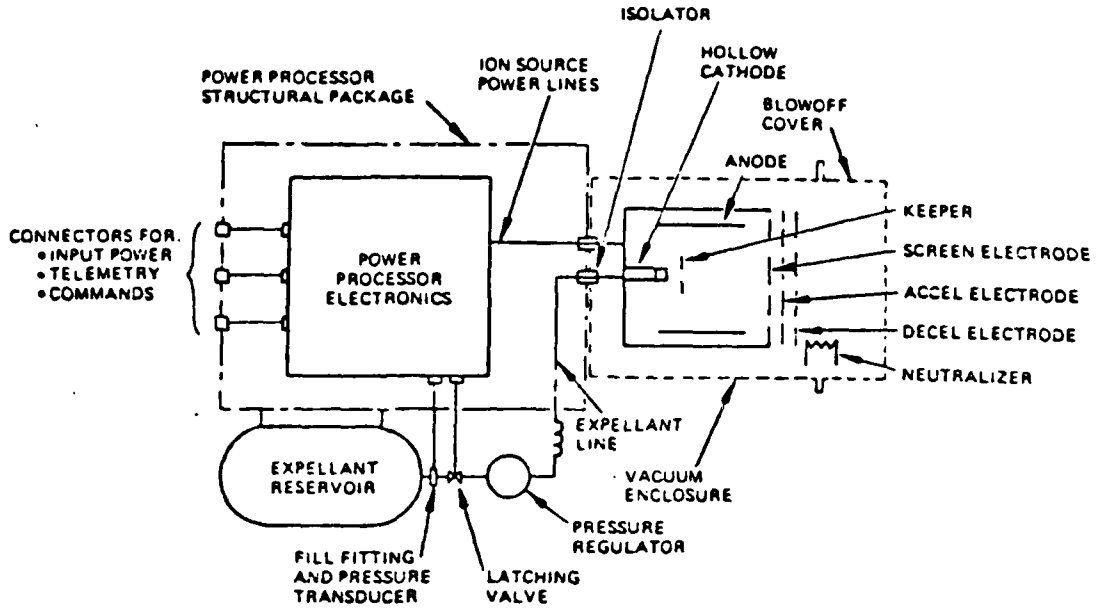

Figure 2. SC4-2 ion gun block diagram.

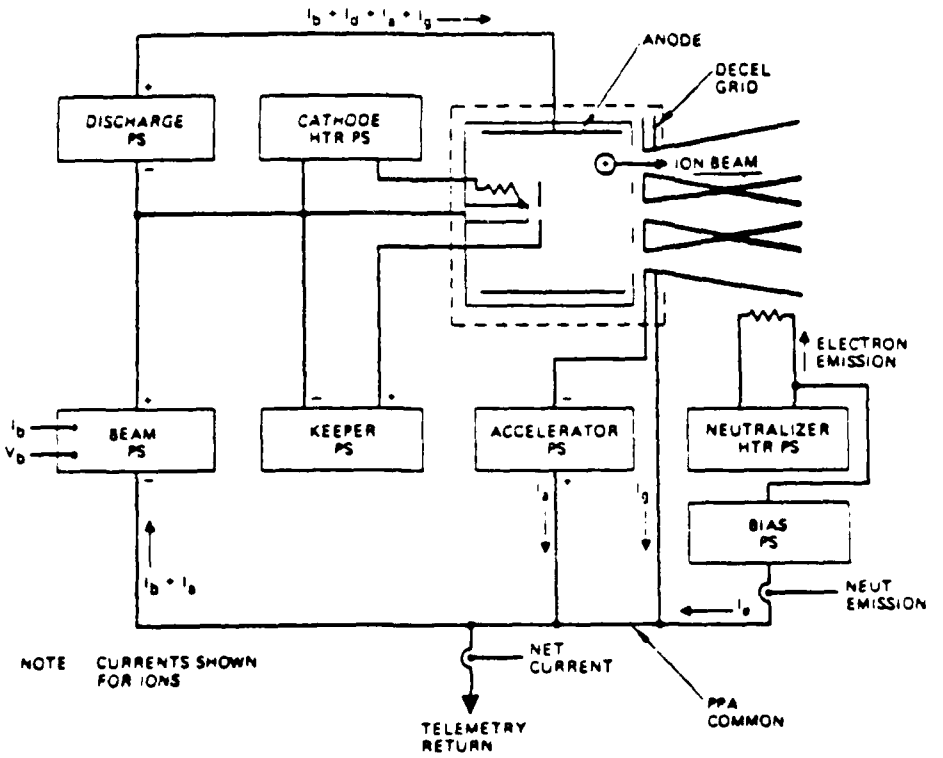

Figure 3. SC4-2 ion gun electrical schematic.

1.3 kHz and a 60 dB dynamic range. Outputs consist of eight narrow band filters and a broadband mode. The narrow band filters have bandwidths of $\pm$ 7.5% and frequencies of 0.4, 1.3, 2.3, 3.0, 10.5, 30, 100 and 300 kHz. In the broadband mode the receiver can be set to cover either the 0 - 3 kHz or 0 - 5 kHz frequency range. (Refs. 14,15)

III. OBSERVATIONS

Three ion gun modes were studied. First, the primary mode for satellite charge control is with both the ion beam and neutralizer on. The satellite is thus emitting a neutralized ion beam. Next, induced (negative) charging experiments were conducted with the ion beam on and the neutralizer off. Only zenon ions are emitted in this mode. Finally, a third mode exists termed 'trickle mode'. In trickle mode the ion beam discharge is on, but without acceleration by the grids. We will look at data taken in each of these three modes.

A. 19 JULY 1979 22:14:00 - 23:14:00 UT

The first example of plasma wave observation during an ion gun experiment comes from 19 July 1979 (Day 200). This example illustrates typical observations for:

- gun off.
- gun and high voltage on, neutralizer off.
- gun on, high voltage and neutralizer off (trickle mode).

The satellite location is near local dusk (1954-2042 LT), between L = 7.6 and 8.0. The electron cyclotron frequency varies from 1.8 kHz to 2.2 kHz. The hydrogen cyclotron frequency is around 1 Hz and the lower hybrid frequency is

about 40 - 50 Hz, and hence these latter two fundamental frequencies are off scale.

The plasma wave data we shall show is primarily in the form of spectrograms. In the spectrograms the horizontal axis is time. The vertical axis is frequency and all of our spectrograms cover a 0 Hz to 4.0 kHz frequency range. Signal strength is indicated using a grey scale. Thus, the spectrogram will be white at frequencies where no signals exist and dark at frequencies where signals are being received. Comparison of signal strength at different frequencies is made by comparing the relative darkness of the spectrogram at those frequencies, with the darker region representing higher signal strength. The plasma wave receiver on the satellite switches antennas every 16 seconds cycling between the electric field antenna and the magnetic field antenna. Hence, the spectrograms cycle between the electric field data and the magnetic field data every 16 seconds. Typical 'gun-off' data are shown in spectrogram form in Figure 4 which covers the period of time 2302:34 to 2303:26. The 19 July 1979 broadband data was taken with the plasma wave receiver in the 0 - 3 kHz mode. The bandwidth in this mode introduces a roll-off at 3 kHz, as seen in the spectrogram. This spectrogram shows the receiver background noise normally present in the magnetic field (B) data. The receiver noise is the resonant response of the receiver to a white noise input, as determined by ground calibration.

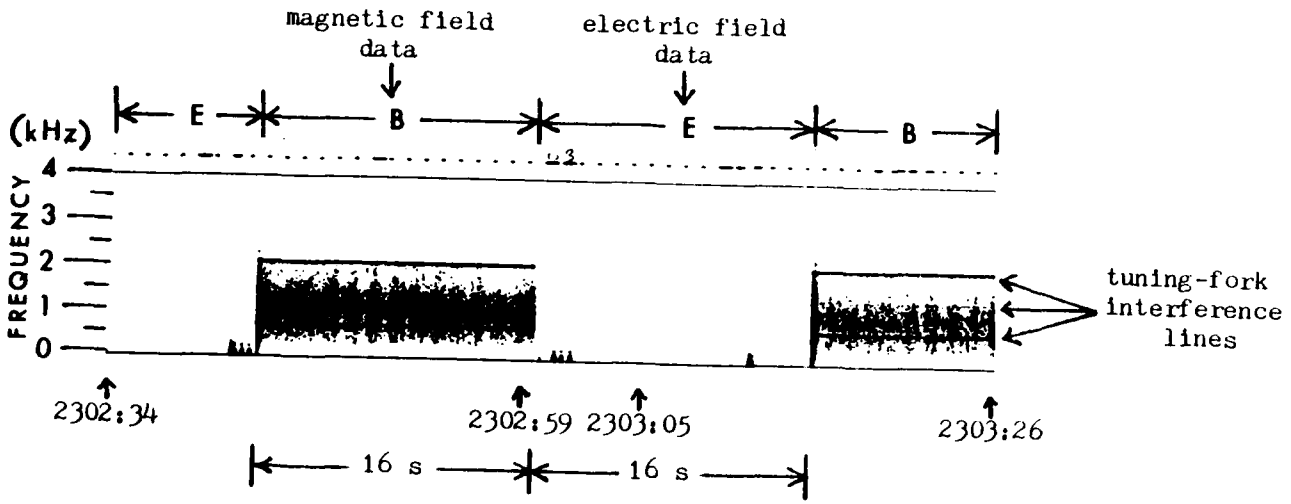

Figure 4. Spectrogram of the period 2302:34 - 2303:26 19 July 19[illegible].

This noise is not visible in the electric field (E) data at the level used to make these spectrograms. Also visible is monochromatic interference at 700 Hz and 2100 Hz and weak interference at 1400 Hz. These signals are caused by a 700 Hz tuning-fork driver circuit in another experiment and are not seen in the electric field data. The next two figures show the features of Figure 4 more clearly. Figure 5 shows a frequency spectrum of the magnetic field data with the gun off taken at 2302:59. Three second averages were used to create the frequency spectrums we shall show. The 700 Hz and 2100 Hz signals are clearly seen to be well above background. Figure 6 shows a frequency spectrum of the electric field data with the gun off taken at 2303:05. Two peaks are found at 2570 Hz and 3155 Hz. The latter signal is probably the electron cyclotron harmonic, or $(3/2)f_{ce}$. The low frequency peak (about 100 Hz) may be an artifact generated on or near the spacecraft. It is near the low frequency cut-off of the receiver band-pass. (Refs. 18,19)

The data set presented below (e.g. the broadband data) began while the ion gun was on with an accelerating voltage of 1 kV and a beam current of 2.0 mA. The neutralizer filament power was off. The satellite was in the dusk bulge region, in a relatively quiet plasma sheet environment. It was uncharged ($< \pm 10$ V) when the gun was off, and charged to approximately -800 V when the gun was on, and unneutralized (Ref. 20). The top panel of Figure 7 is a spectrogram

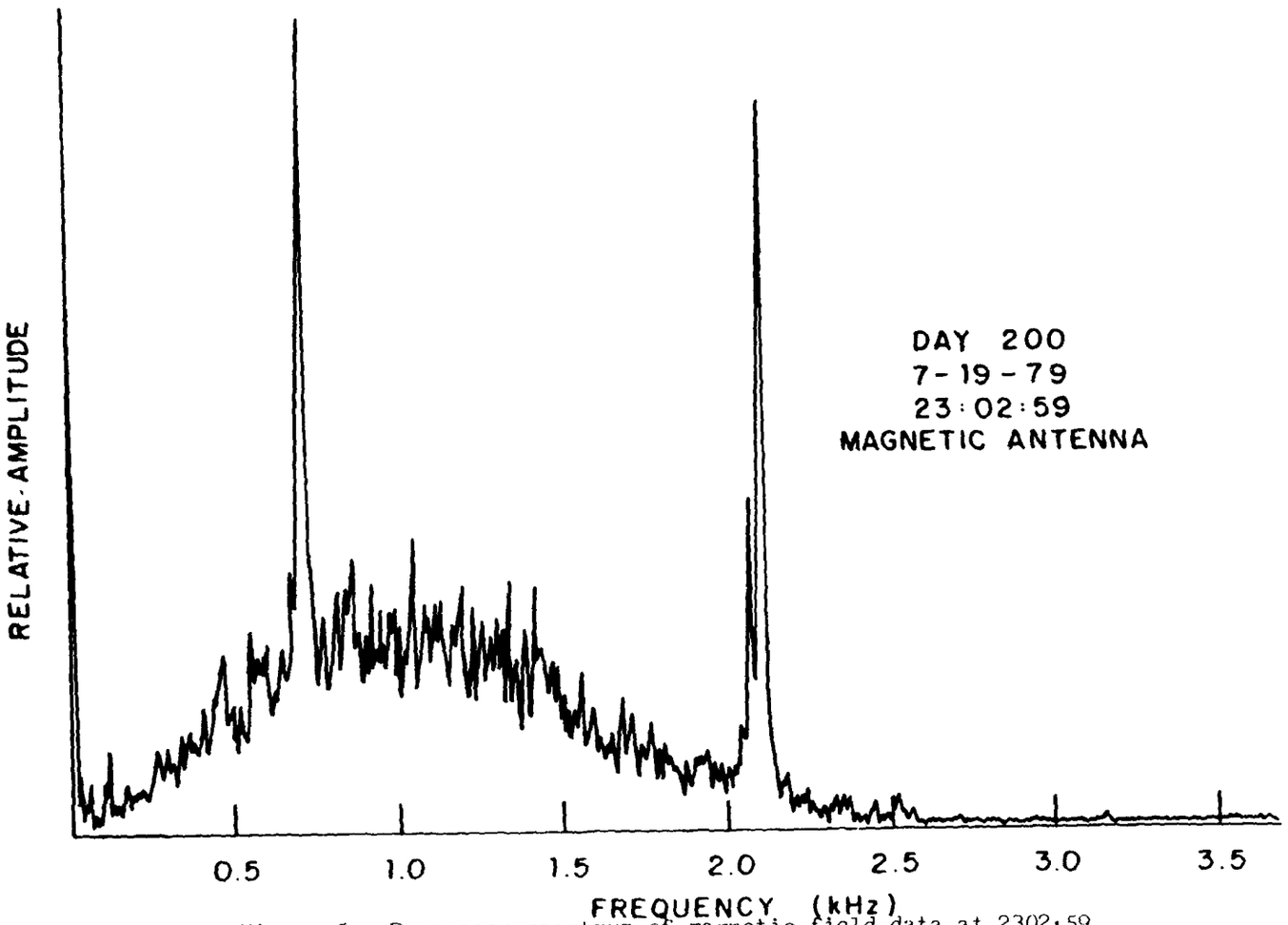

Figure 5. Frequency spectrum of magnetic field data at 2302:59 19 July 1979 using 3 second averaging.

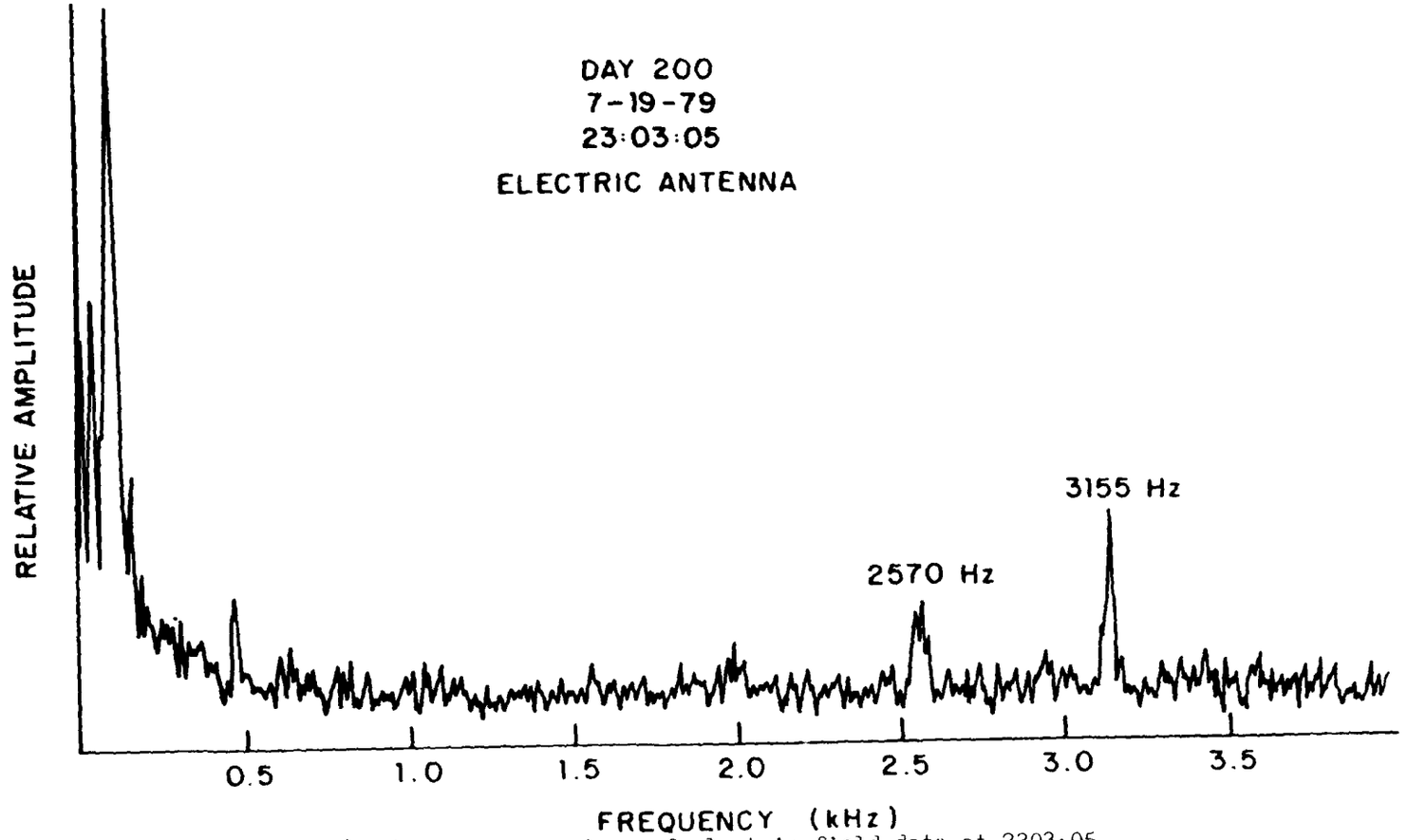

Figure 6. Frequency spectrum of electric field data at 2303:05 19 July 1979 using 3 second averaging.

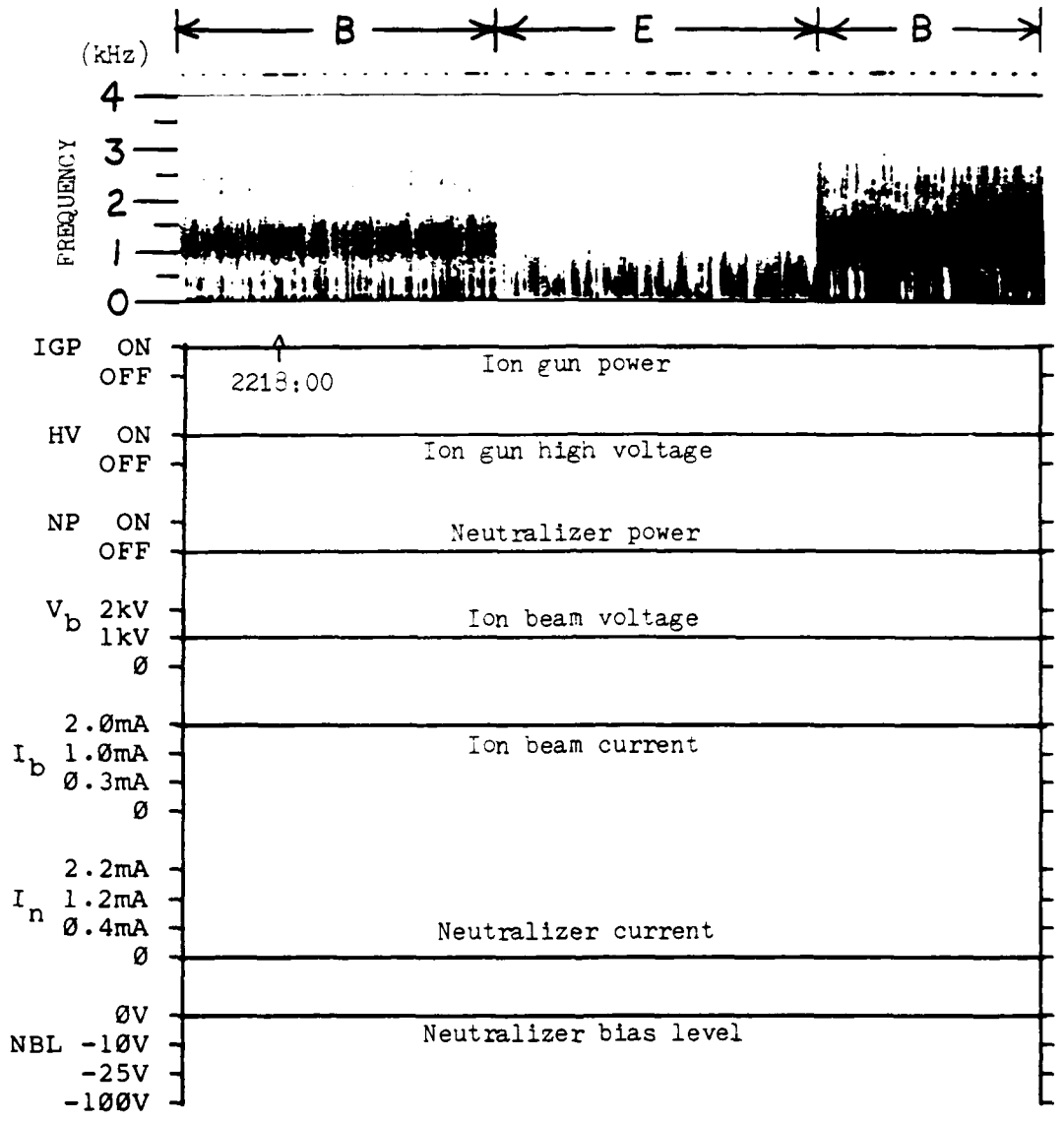

Figure 7. Spectrogram of the period 2217:55 - 2218:38 19 July 1979.

showing about 43 seconds of plasma wave data for this ion gun operating mode. Also shown in Figure 7 are the ion gun mode settings. These include ion gun power (IGP), high voltage (HV), neutralizer power (NP), ion beam voltage (V_b), ion beam current (I_b), neutralizer current (I_n), and neutralizer bias level (NBL). Again, the receiver was switched every 16 seconds and the roll-off at 3 kHz is due to the receiver mode. There is a broad maximum from 1.0 to 1.5 kHz visible in the magnetic field data as shown by the darkening of the spectrogram at those frequencies. This signal is not present in the electric field data. Brief, vertical striations in the data, particularly the magnetic data, show a broad spectrum which we interpret as the signal generated by arcing on or in the satellite. The vertical striations are obviously due to pulses with periods considerably less than a second. The frequency spectrum is analyzed in more detail in the following two figures. Figure 8 is a frequency spectrum of the magnetic field data at 2218. The spiky elements attributed to arcing have largely been averaged out by three second averaging. Figure 8 shows that the most intense average signals are below 500 Hz, followed by a broad peak from 1.1 - 1.4 kHz. This latter peak is the broad maximum visible in the spectrogram and is similar to the receiver noise signal shown in Figure 5. Consideration of calibrated filter data (below) show that this signal is orders of magnitude higher in amplitude than

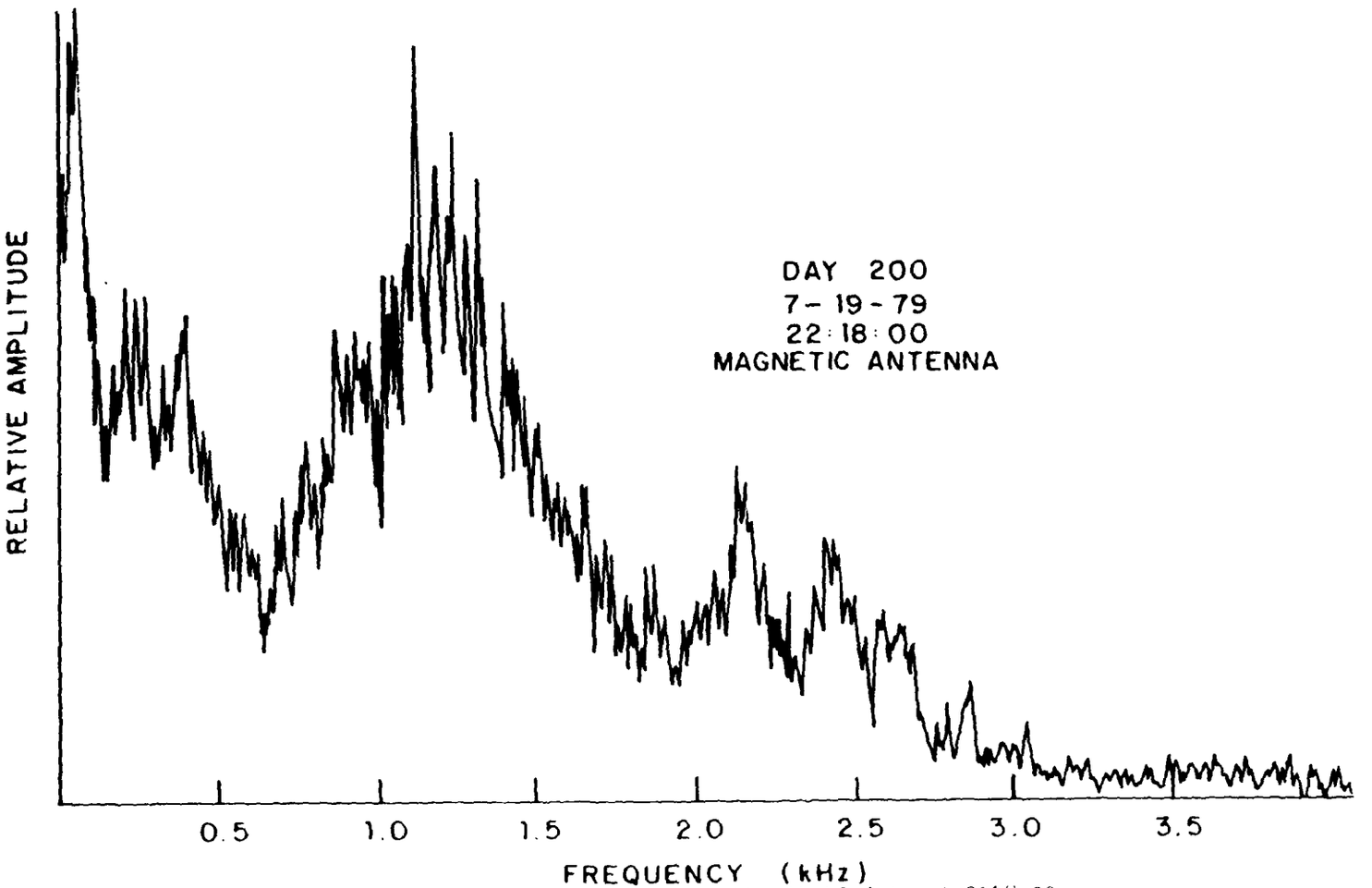

Figure 8. Frequency spectrum of magnetic field data at 2218:00 19 July 1979 using 3 second averaging.

background noise. This appears to be, therefore, the receiver response to an intense white noise input signal. Figure 9 is a frequency spectrum of the electric field data at 2218:15. A broad signal, from near zero to about 1.5 kHz, monotonically decreasing in amplitude is seen in Figure 9 but was not present in the gun-off data of Figure 6. The smaller peaks near 2.5 kHz and 3.1 kHz are still visible. The low frequency spectrum is similar to that found in the magnetic field data of Figure 8, but, again there is no signal in the 1.Ø - 1.4 kHz region of the electric field data as there is in the magnetic field data. The small peak at 3.1 kHz is again thought to be the $(3/2)f_{ce}$ signal (f_{ce} = 2.1 kHz at this time, as calculated from SC11 data).

At 2226:55 the high voltage is turned off resulting in trickle mode. A net current of 1Ø - 2Ø microamps is still being emitted (according to gun diagnostics). The result of this ion emission is a satellite potential near zero ($< \pm 1Ø$ V). The arcing seen in Figure 7 ceases during an electric field measurement as shown by Figure 1Ø. Still visible during trickle mode is the broad maximum from 1.Ø - 1.5 kHz in the magnetic field data. Calibrated filter data still show substantial enhancement over receiver background. The intense low frequency (near 1ØØ Hz) signal in the electric field data present with the gun off, and the gun on, remains visible. The signals become clearer over the next few

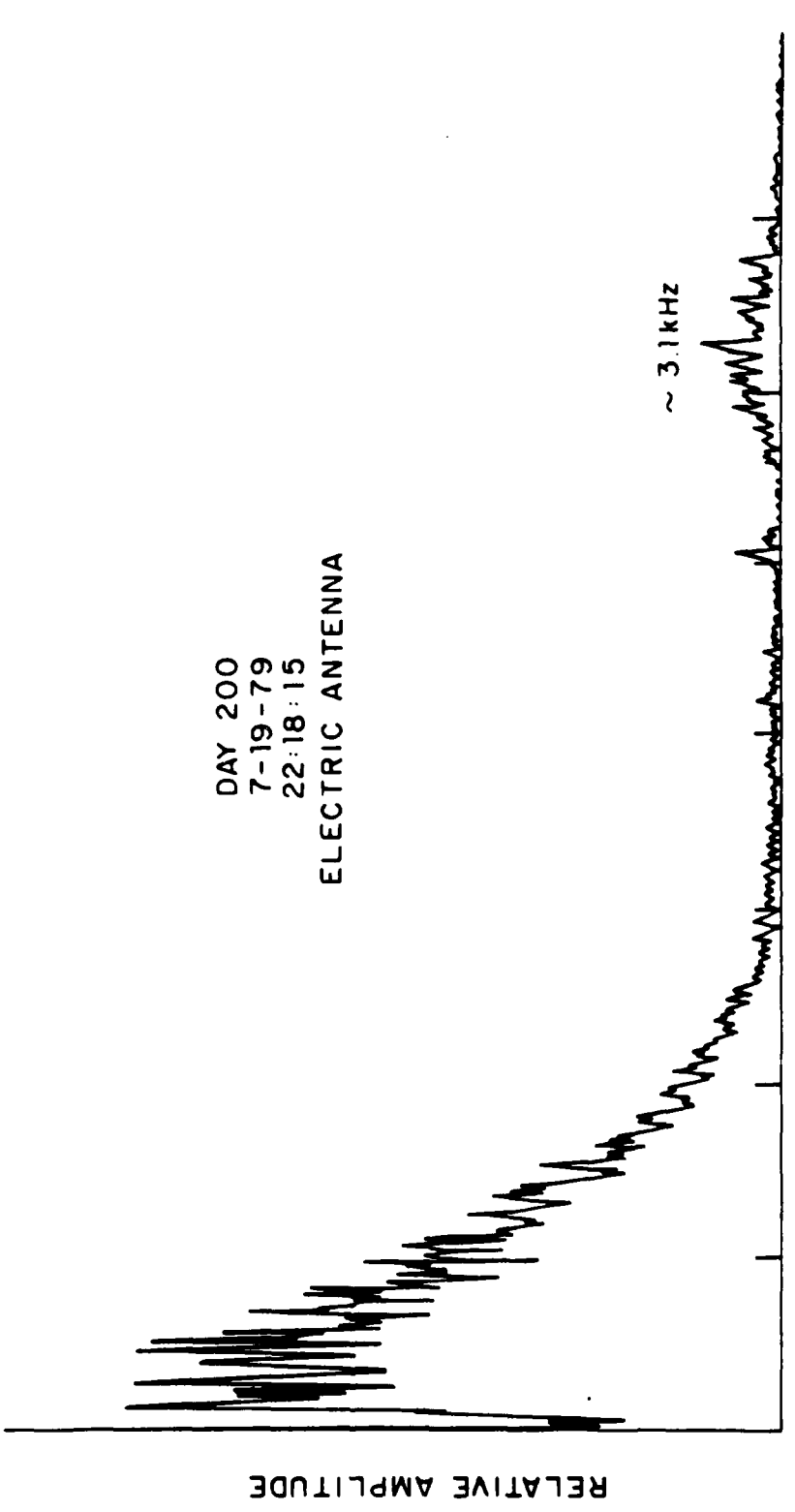

Figure 9. Frequency spectrum of electric field data at 2218:15 19 July 1979 using 3 second averaging.

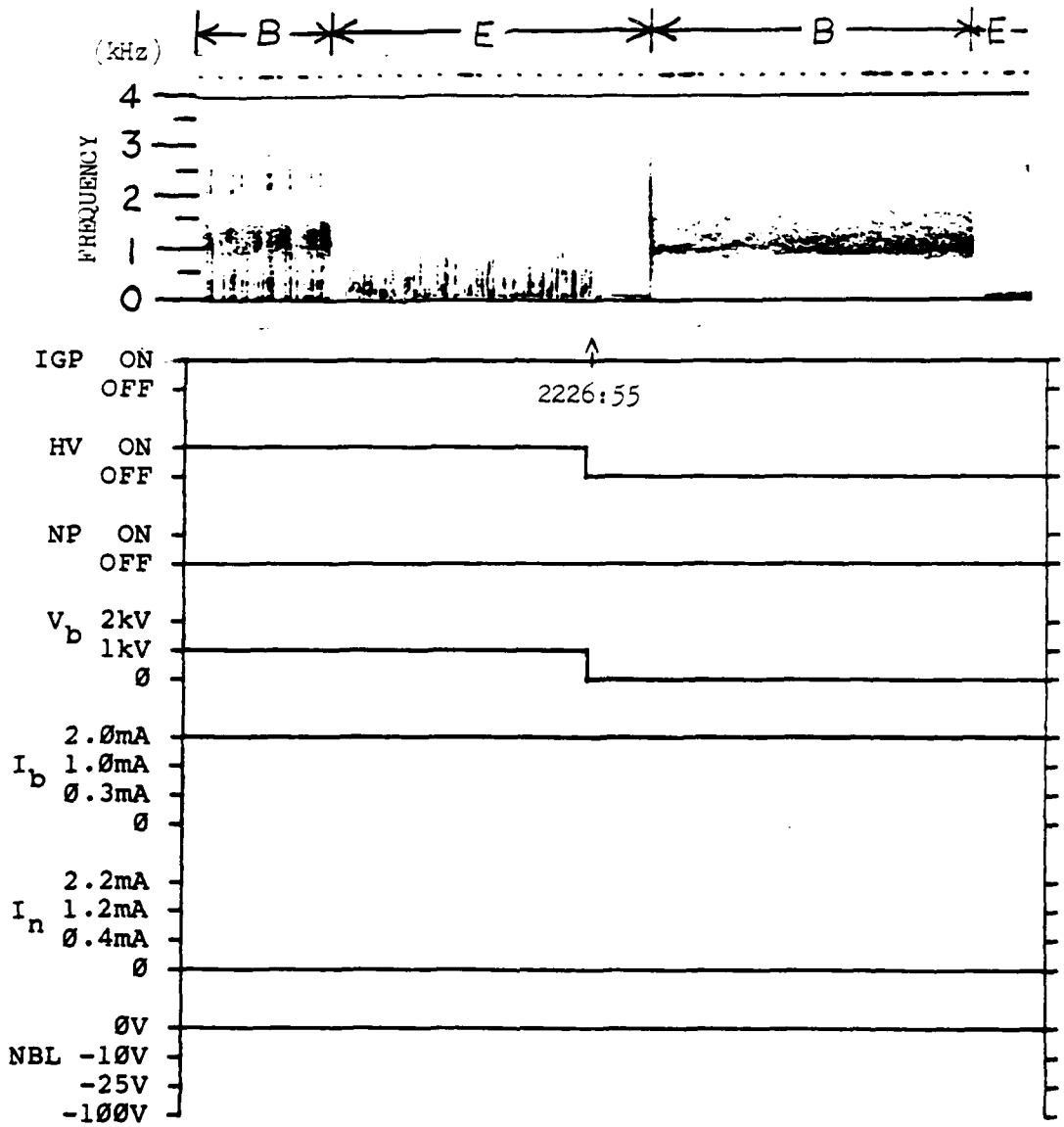

Figure 10. Spectrogram of the period 2226:36 - 2227:18 19 July 1979.

minutes. Figure 11 shows that at 2229 both the broadband signal in the magnetic field data and the very low frequency signal in the electric field data have become more intense, but have not substantially changed in character. There is a narrow signal now visible at about 1.2 kHz in the electric field data. This latter signal is not generally visible during this period. We interpret this signal as being natural because of its finite width and variation in frequency. Figure 12 is a frequency spectrum of the electric field data at 2228:53. The intense signal from near zero to about 200 Hz remains, with several additional narrow peaks up to about 500 Hz. Also the line spectrum shows the feature seen in Figure 11 at 1190 Hz, and an additional peak exists at 3.16 kHz (again $(3/2)f_{ce}$). The apparent weakness of the 3.16 kHz signal is partly due to receiver roll-off in this mode. Figure 13 is a frequency spectrum for the magnetic field data at 2229:45. The broad peak from 1.0 - 1.5 kHz is similar to that found previously; that is, similar to the receiver resonance response to a white noise input. The lower frequency peak (below 500 Hz) seen in Figure 8 is now gone. Hence the low frequency peak must nominally be associated with the accelerated beam in the plasma, while the broad peak (white noise) is most likely induced by interactions between the cold, dense gun plasma and ambient plasma. To illustrate this graphically, Figure 14(a) shows a velocity distribution for an accelerated Xe^+

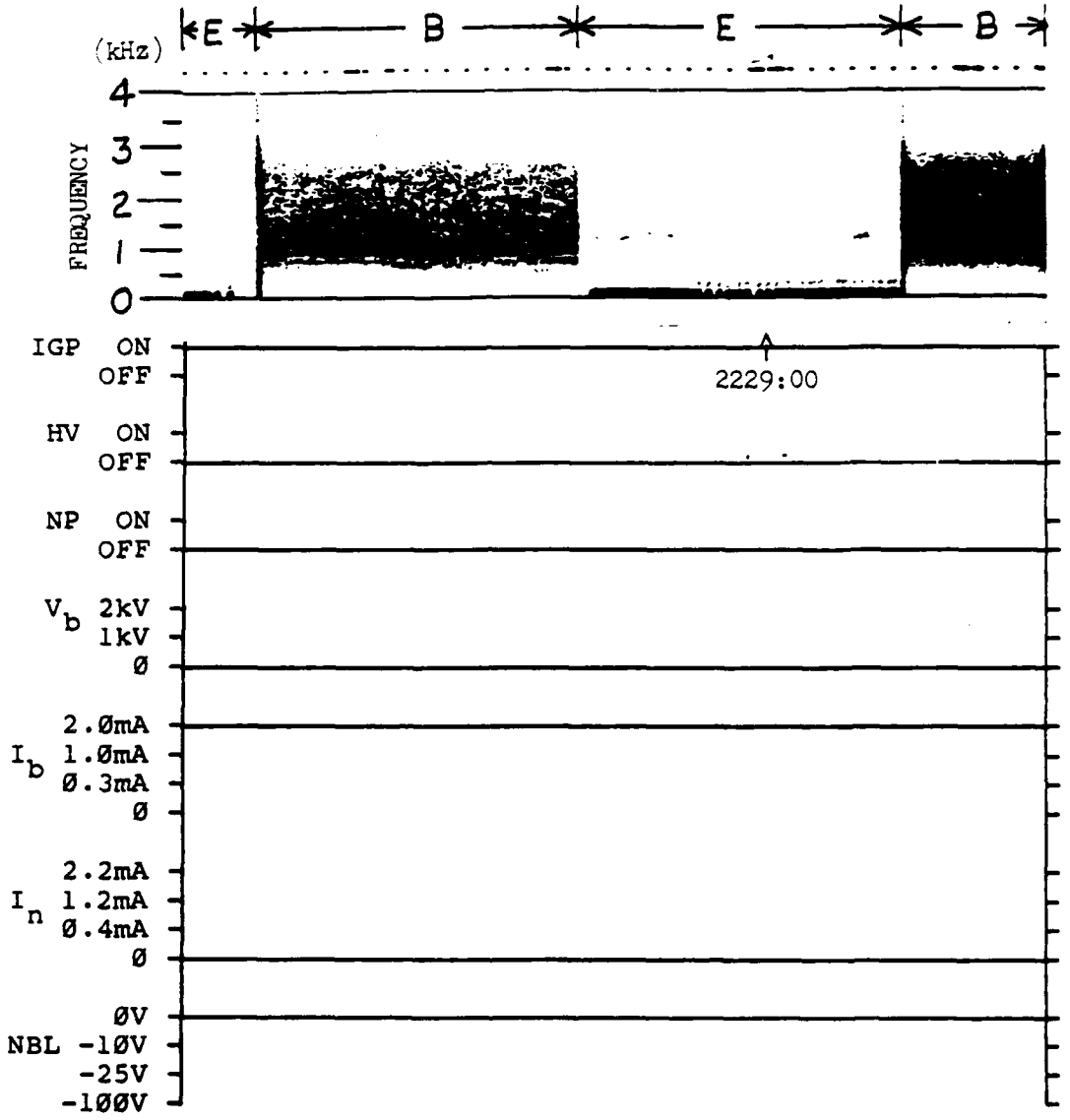

Figure 11. Spectrogram of the period 2228:30 - 2229:14 19 July 1979.

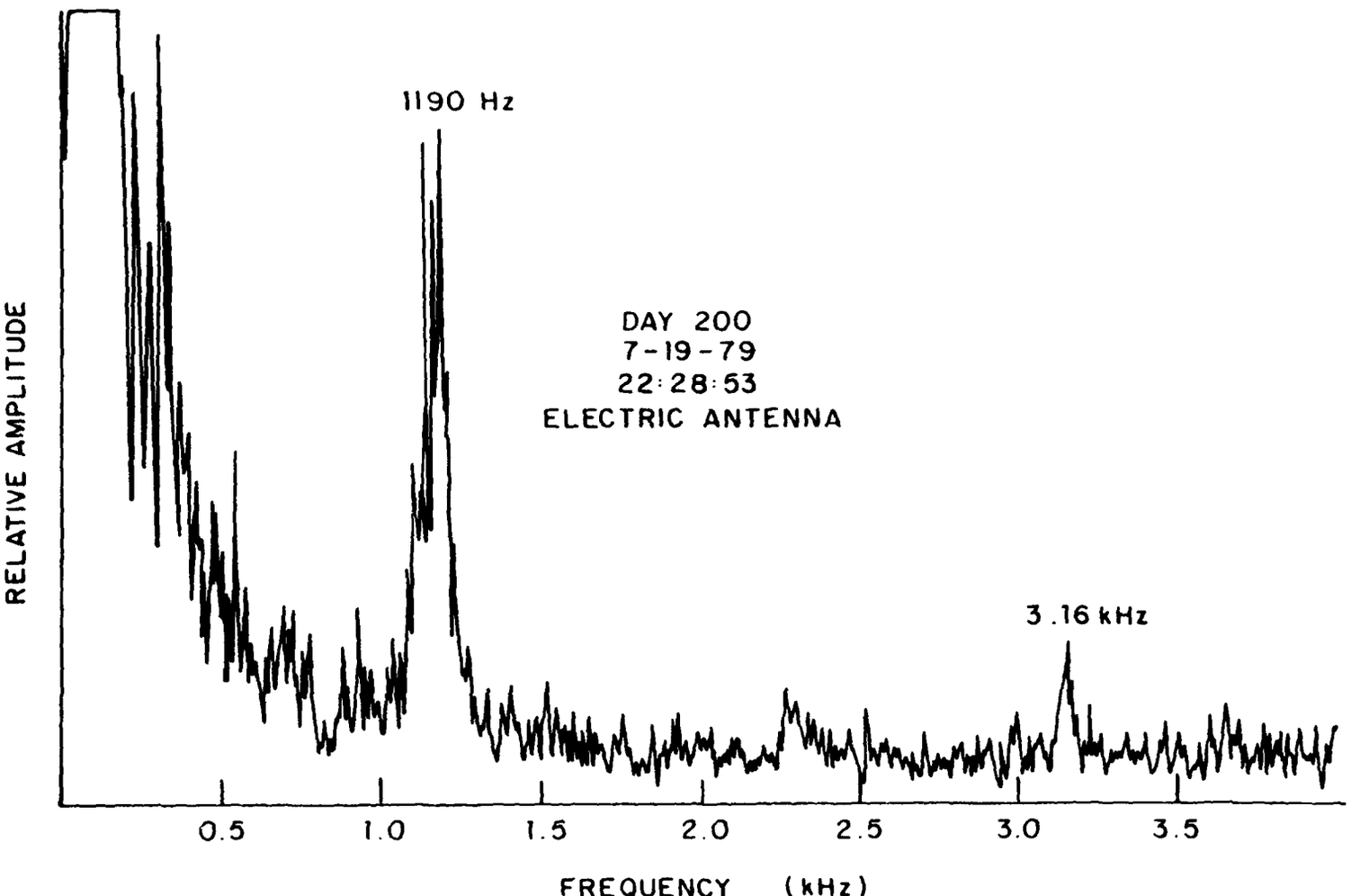

Figure 12. Frequency spectrum of electric field data at 2228:53 19 July 1979 using 3 second averaging.

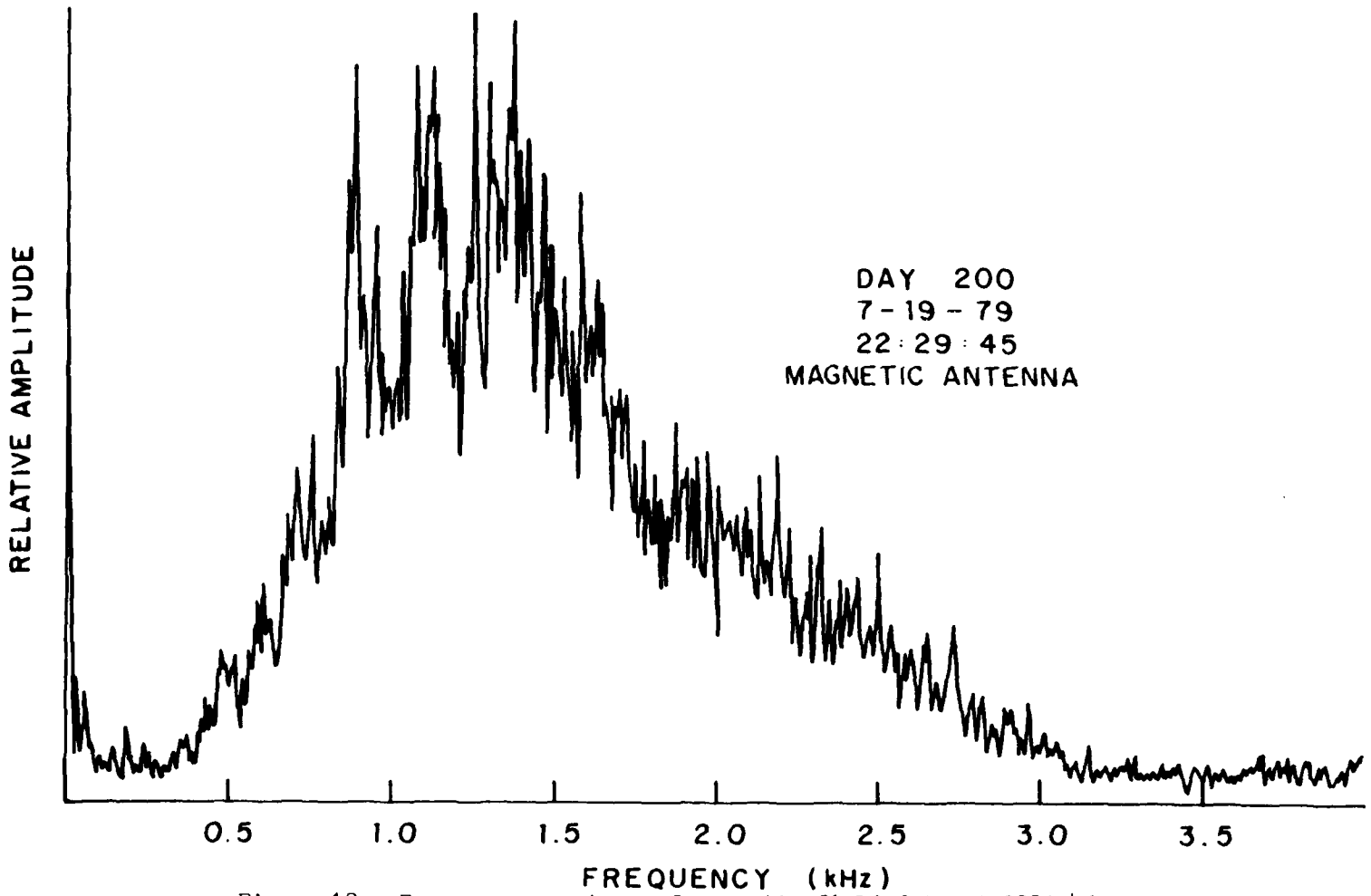

Figure 13. Frequency spectrum of magnetic field data at 2229:45 19 July 1979 using 3 second averaging.

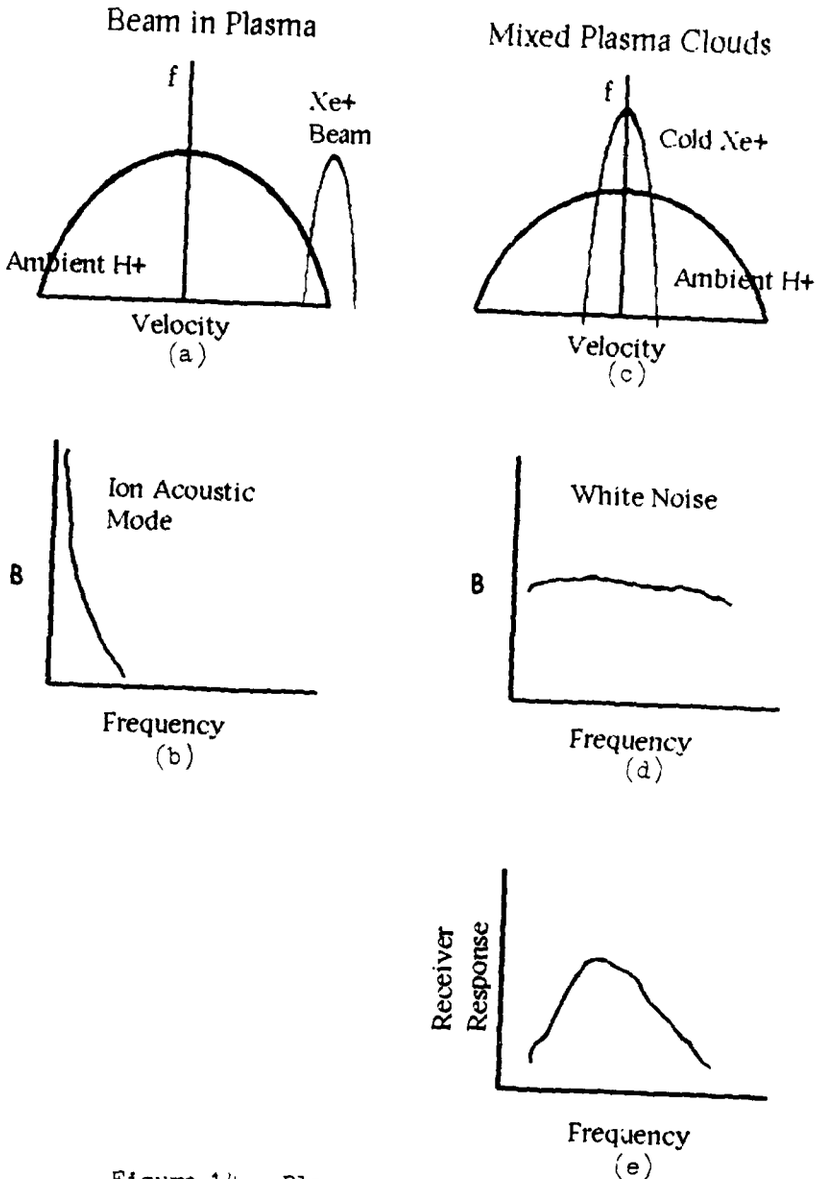

Figure 14. Plasma waves generated by beam-plasma interactions.

beam in a cold H^+ plasma. A possible result of this instability is waves in the ion acoustic mode with a frequency distribution as shown in Figure 14(b) (Refs. 21,22). Similarly, Figure 14(c) shows a velocity distribution for a cold Xe^+ cloud in a cold H^+ plasma. It is likely that this distribution is also unstable. We suggest that the result is a spectrum of nearly constant amplitude over a wide frequency range (white noise) as shown in Figure 14(d). Again, a white noise signal is known to produce a receiver response as shown in Figure 14(e). The magnetic field data have cleaned up substantially and in particular, the 700 Hz and 2100 Hz lines are not visible. It is now clear that this is because more intense signals have driven the AGC down, and these relatively weak markers are now below the noise level. At 2232:03 (not shown) the high voltage is turned back on. The arcing resumes, and the data resume their former character. The signals do appear more intense in the spectrogram (not shown), but this is partly an artifact of AGC and processing variations. The AGC may be driven by a different portion of the frequency spectrum during this latter period. This could reflect different characteristics of differential charging following the trickle mode induced discharge of the dielectric materials (Ref. 23).

There are changes in the data which are independent of gun status change. Figure 15 shows that at 2234:04 there is

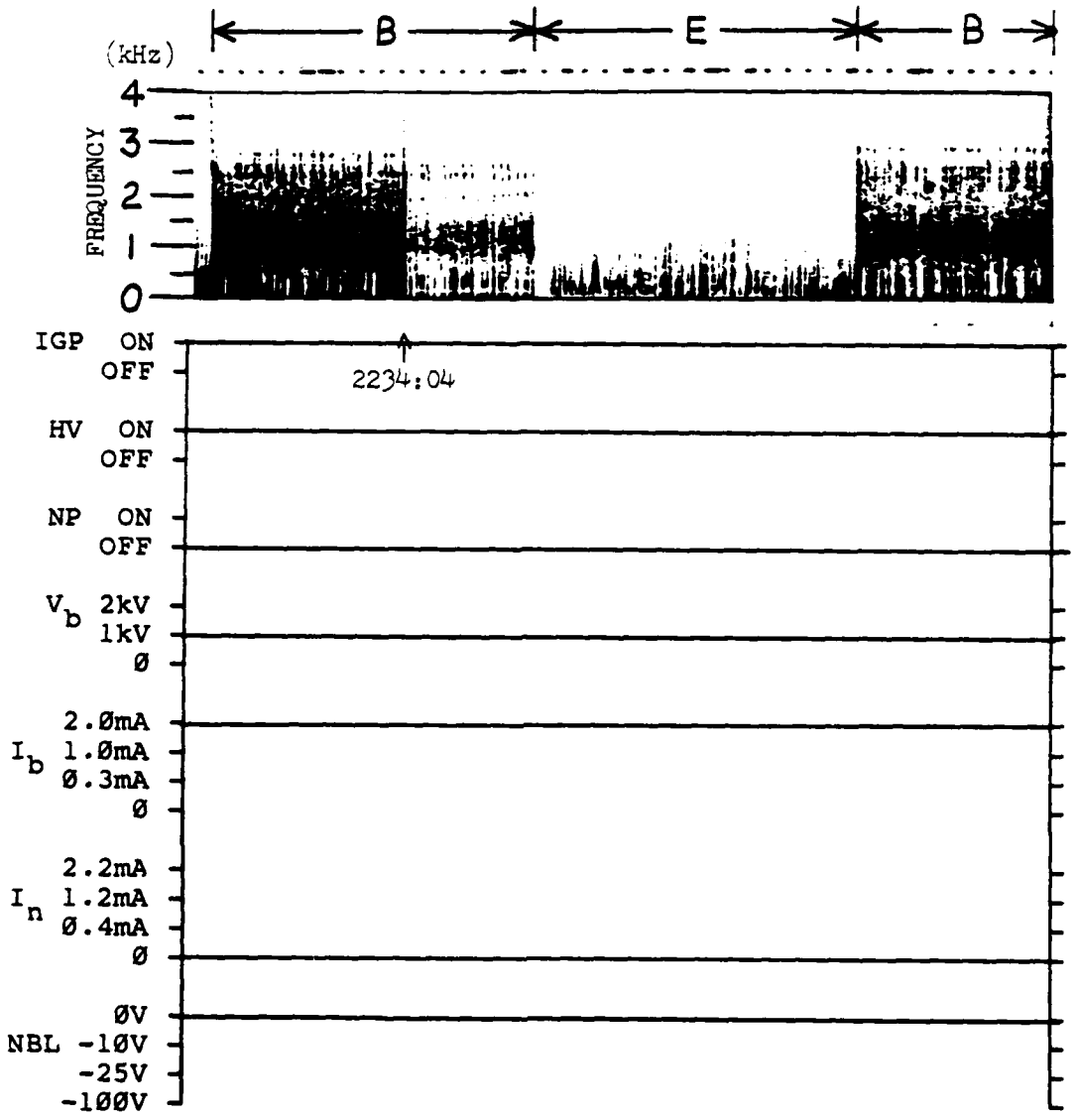

Figure 15. Spectrogram of the period 2233:56 - 2234:37 19 July 1979.

a sharp change in intensities which is independent of any changes in the ion gun status. The spectrum is largely unchanged, however. Examination of the narrowband filter data (shown below) reveals that this amplitude change occurs in the .4 kHz - 3.Ø kHz channels of the electric field data after both trickle mode operations. When high voltage is turned on, the electric field data in the Ø.4 - 3.Ø kHz range peak briefly approximately 5 to 1Ø dB above the 'steady state' gun-on levels. The transient period lasts about one to two minutes (one to two spin periods).

Changes in the gun operating mode changed the plasma wave data. At 2258:Ø6 the beam current is decreased to 1.Ø mA and at 23ØØ:22 the beam current is decreased to Ø.3 mA. Each decrease in beam current caused the arcing signals (vertical striations) to decrease in intensity, and frequency of occurrence. Figure 16 shows data at Ø.3 mA beam current. The spikes that indicate arcing are seen to be less intense and fewer in number per each 16 second window than they were at 2.Ø mA beam current. All other characteristics of the spectrum remain the same. At 23Ø1:39 all ion gun power is turned off. Figure 16 shows that arcing ceases and the the 7ØØ, 14ØØ and 21ØØ Hz interference lines are again visible.

The operation is summarized in Figure 17. The narrowband filter data for the period 213Ø - 233Ø UT is shown for both antennas. Trickle mode operations were

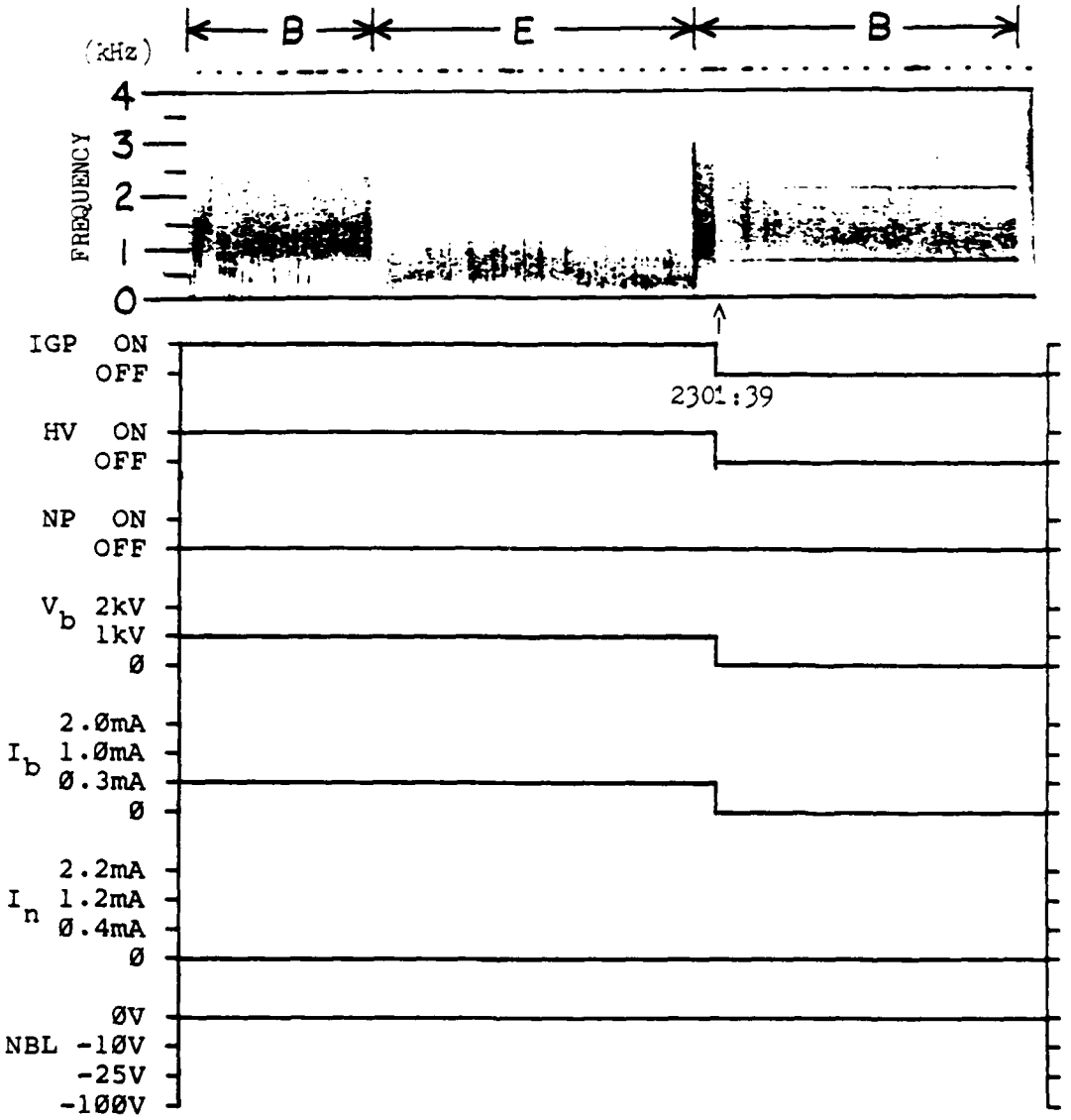

Figure 16. Spectrogram of the period 2301:09 - 2301:55 19 July 1979.

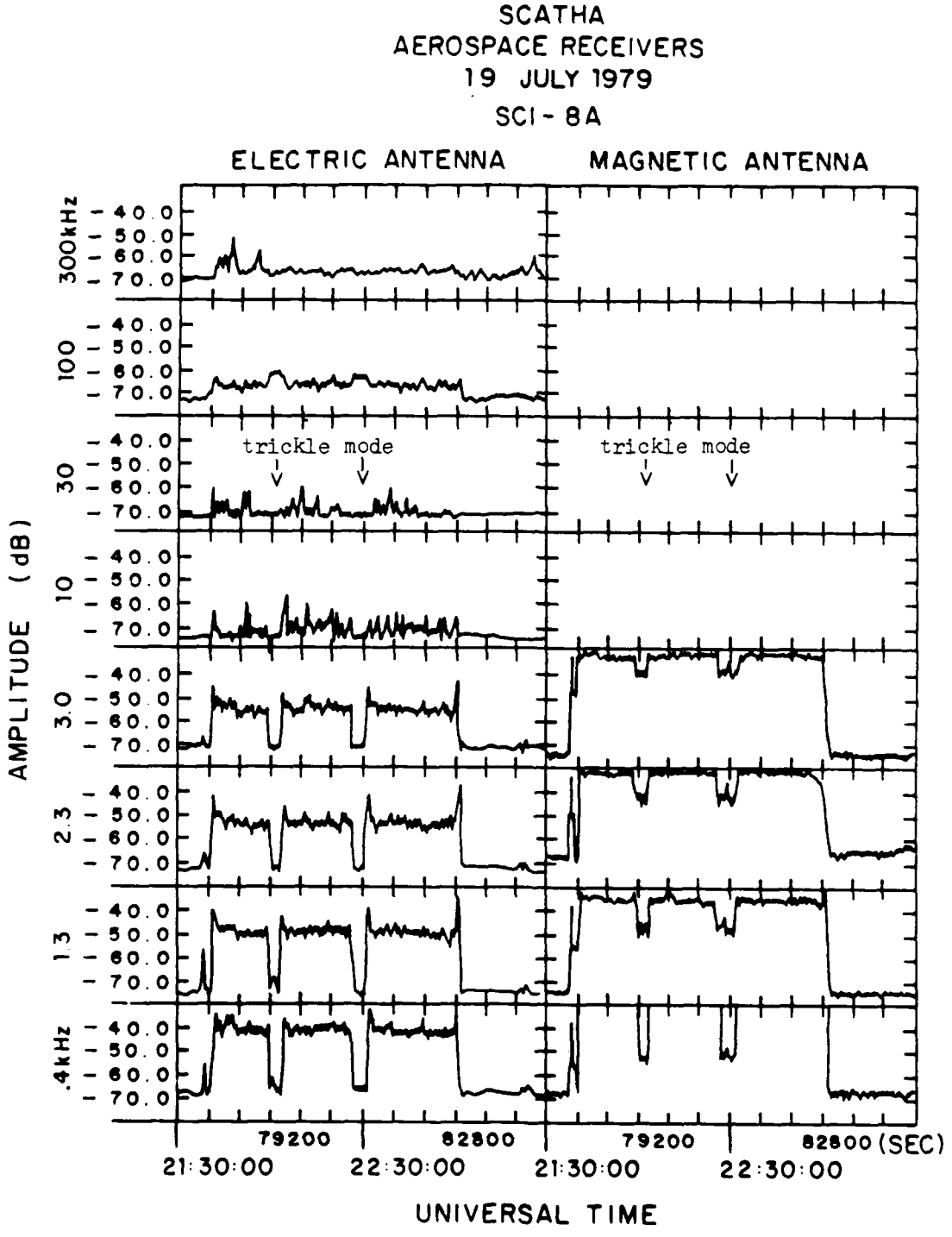

Figure 17. Narrowband filter data for 2130 - 2330 19 July 1979.

conducted from 2159:06 to 2203:35 as well as the 2226:55 to 2232:03 period. Both periods are clearly seen on the 0.4, 1.3, 2.3 and 3.0 kHz channels of both antennas. The electric field data show 20 - 30 dB increases in amplitude in the 400 Hz to 3.0 kHz range with the ion beam on. The amplitudes return to near background values during trickle mode. The magnetic field data shows that at 400 Hz the amplitude increase is greater than 40 dB and the signal peaks off the scale. The 1.3 - 3.0 kHz channels show magnetic field amplitude increases of 35 - 40 dB. During trickle mode the magnetic field amplitudes show a decrease, but remain 15 - 30 dB above background. We interpret this as showing that no interference generated at these frequencies by the gun during trickle mode reaches the electric antenna, but that an electrostatic or electromagnetic signal is caused by the interaction of the 'dense' xenon plasma from the gun with the ambient plasma in the immediate vicinity (a few meters) of the satellite, and this signal is observed by the magnetic loop antenna. The 100 kHz electric field channel shows an increase in signal strength during trickle mode. This frequency is comparable to the upper hybrid resonance or the plasma frequency near the satellite.

B. 2 APRIL 1979 1513 - 1548 UT

The second operation we shall present occurs in eclipse on Day 92 of 1979. Plasma wave response to gun operations appear similar to those observed in the dusk bulge region on day 200. This example illustrates typical observations for:

- gun, high voltage and neutralizer on.
- gun and high voltage on, neutralizer off.
- gun on, high voltage and neutralizer off (trickle mode).
- gun off.

During this period the satellite is between L = 7.3 and 7.6 and the time is just after local midnight. The satellite is in eclipse from 1430:00 - 1537:53. The electron cyclotron frequency varies from 3.2 to 3.6 kHz, the hydrogen cyclotron frequency is about 2 Hz, and the lower hybrid frequency varies from 75 to 85 Hz. Only the spectrograms and narrowband data for this period are shown. Attempts to generate amplitude plots for the frequency spectrum were not successful because of the age of the magnetic tape on which the data was stored. The data for this period was taken in the 0 - 5 kHz receiver mode, but only 0 - 4 kHz is shown. Therefore, no receiver roll-off at 3 kHz occurs for this data.

This data set begins with the ion beam on with beam voltage at 1 kV and beam current at 1.0 mA; neutralizer on with neutralizer current at 1.2 mA and the neutralizer bias

level at -1Ø V. Hence, there is a net positive current to the spacecraft, and it charges positively. The magnetic field data in Figure 18 show a continuous band of signals from just below 1 kHz to the top of the spectrogram at 4 kHz with the 1 kHz - 2 kHz region showing slightly greater signal strength. The 7ØØ Hz and 21ØØ Hz interference lines are not visible. A faint spectrum exists in the electric field data from Ø.4 - 1.5 kHz. This diffuse spectrum is regularly seen during such neutralized beam operations. Examination of filter data (presented below) show that this signal amplitude has increased relative to the gun off data (also presented below).

Figure 19 shows how arcing occurs with the neutralizer off (neutralizer off at 1517:47). This data resembles the data from Day 2ØØ at the same gun settings. The broad frequency spikes and the intense 1.Ø - 1.5 kHz band are both present in the magnetic field data. The electric field data appear similar to the arcing data shown for day 2ØØ. Figure 2Ø shows data taken as the high voltage is turned off at 1518:5Ø. The gun enters trickle mode at that point. (Note that I_b = 1.Ø mA reflects the beam discharge current setting, and hence ionization rate in the chamber. The emitted current is only 1Ø - 2Ø microamps). Visible at this time in the magnetic field data are the 7ØØ, 14ØØ and 21ØØ Hz interference lines and the diffuse background noise. The electric field data contains a very low frequency (less than

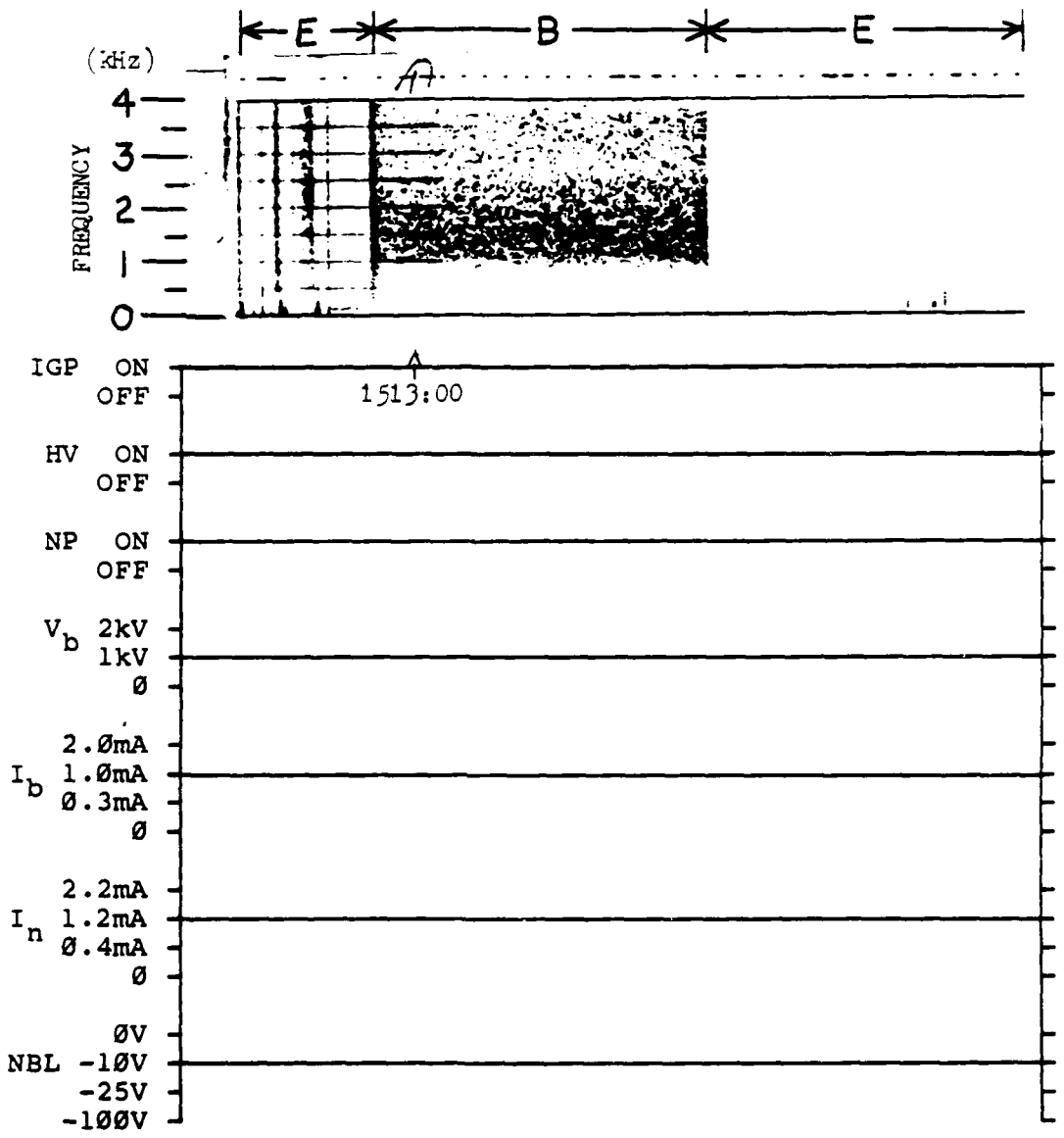

Figure 18. Spectrogram of the period 1512:54 - 1513:28 2 April 1979.

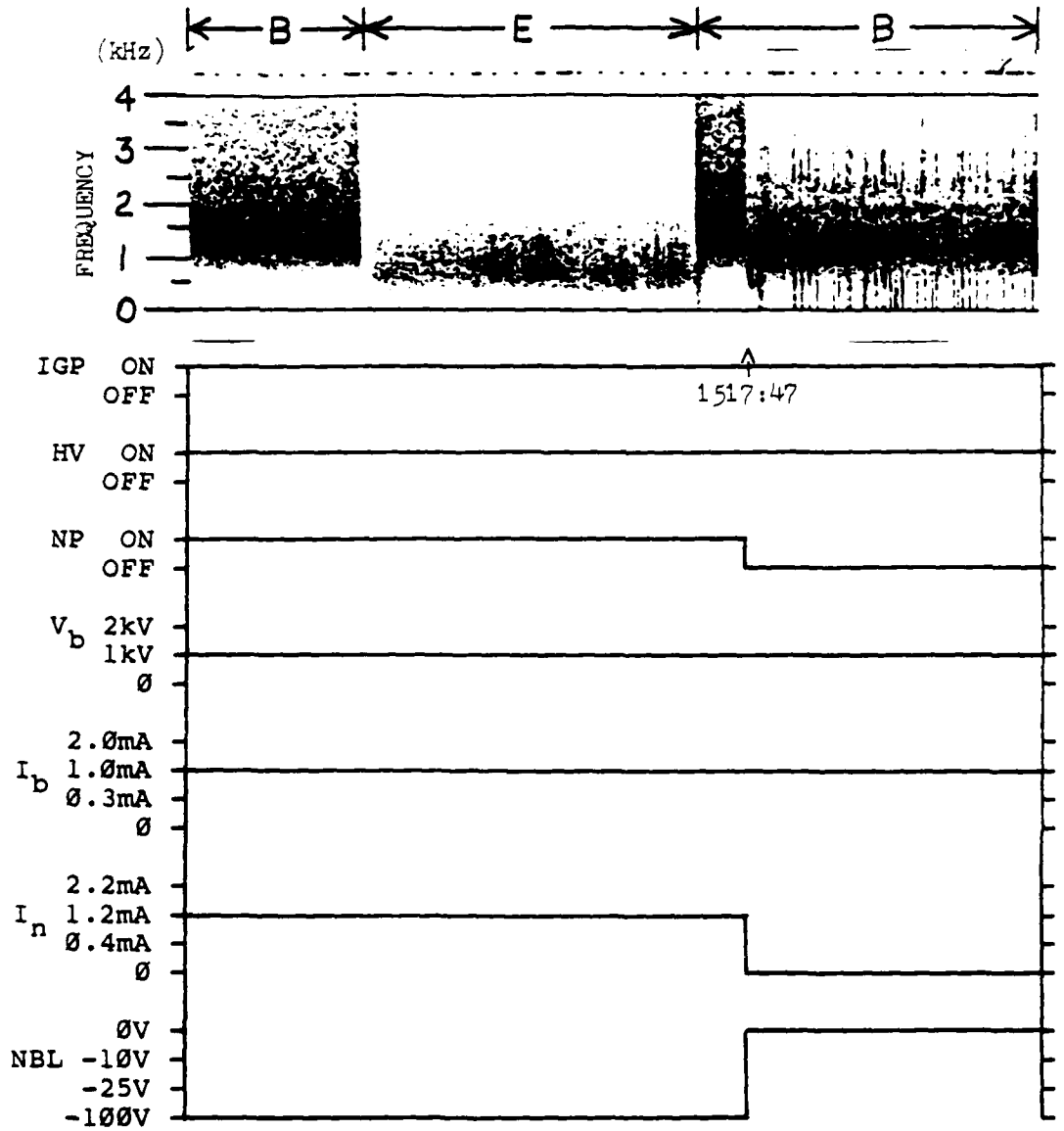

Figure 19. Spectrogram of the period 1517:22 - 1518:02 2 April 1979.

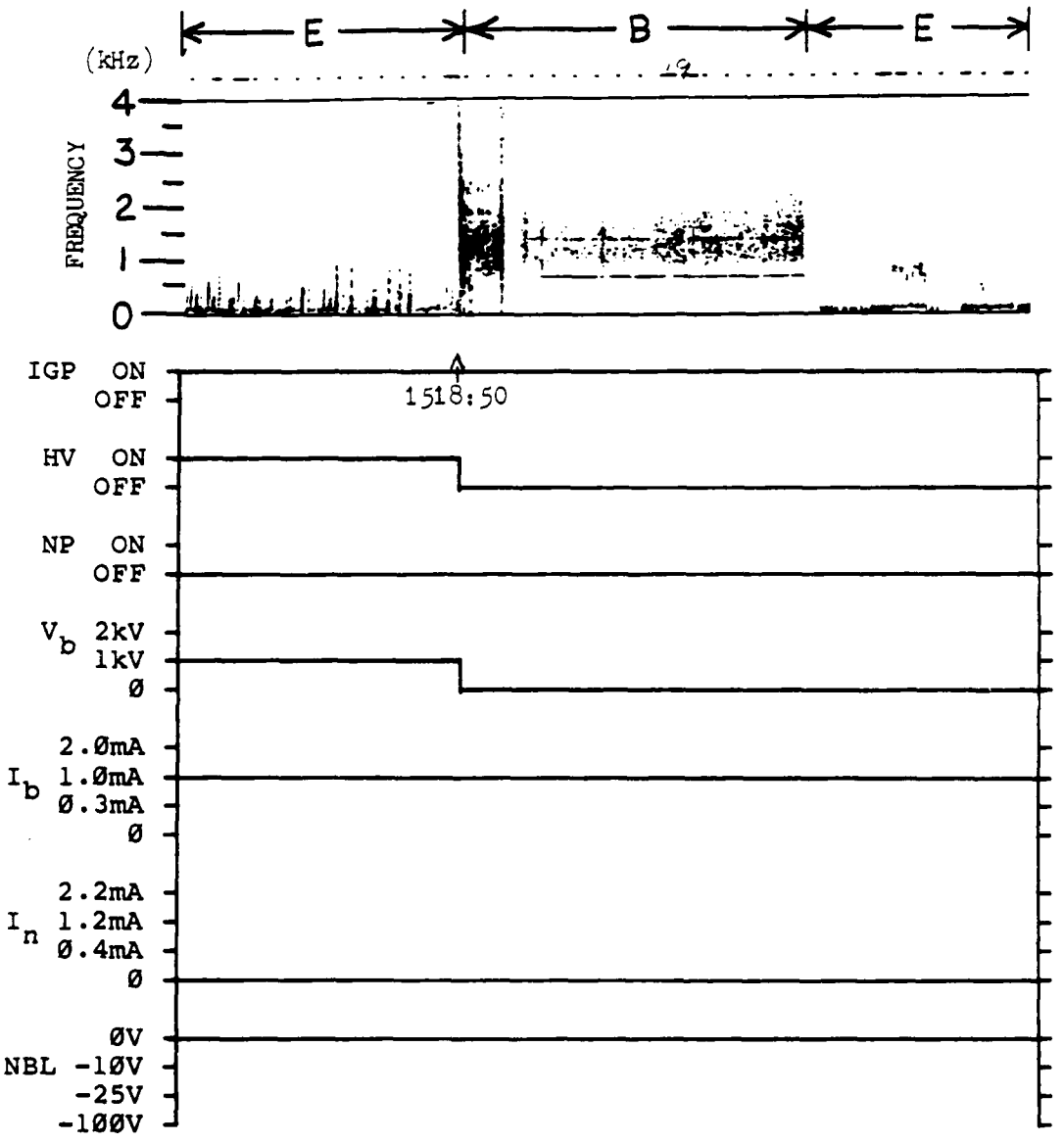

Figure 20. Spectrogram of the period 1518:37 - 1519:16 2 April 1979.

100 Hz) signal and some spotty signals near one kHz. Figure 21 shows further fluctuations in the electric field data which are apparently due to ambient plasma waves. The magnetic field data continue to show the broad, diffuse spectrum. The 700 Hz interference line is barely visible, while the 1400 and 2100 Hz lines can no longer be seen. Since these signals are presumably of constant amplitude, their disappearance could again be caused by changes in the broad background amplitude or by attenuation of the signals in the xenon plasma cloud around the satellite. Figure 21 also shows that arcing resumes when the high voltage is turned on at 1520:05. The characteristics of the electric and magnetic field data are similar to those already presented for arcing. The arcing signature ceases in Figure 22 a few seconds after the 1521:15 turn on of the neutralizer at 1.2 mA and bias level -100 V. (Note time delay may be due to an error in the command log as this delay is not seen in similar data). The characteristics of the field data is now the same as in Figure 18. Neutralizer bias level changes made during neutral beam emission have shown almost no effect on the plasma wave data. Four bias level changes were made during the time period we are presenting here. In all four cases there was no detectable change in the magnetic field data. Plasma wave data during a bias level change from -100 V to 0 V is shown in Figure 23. The electric field data now shows some fine structure.

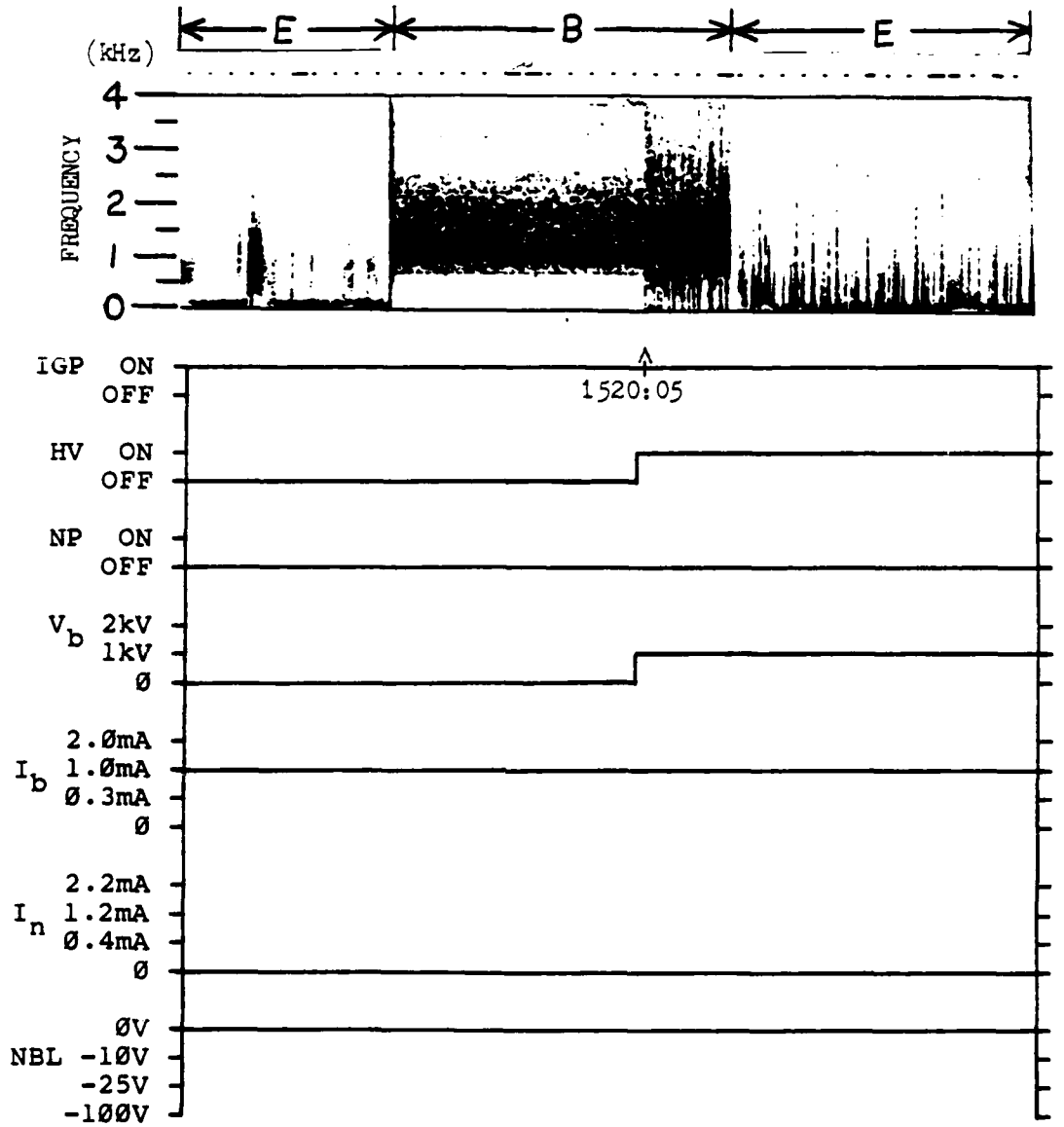

Figure 21. Spectrogram of the period 1519:44 - 1520:24 2 April 1979.

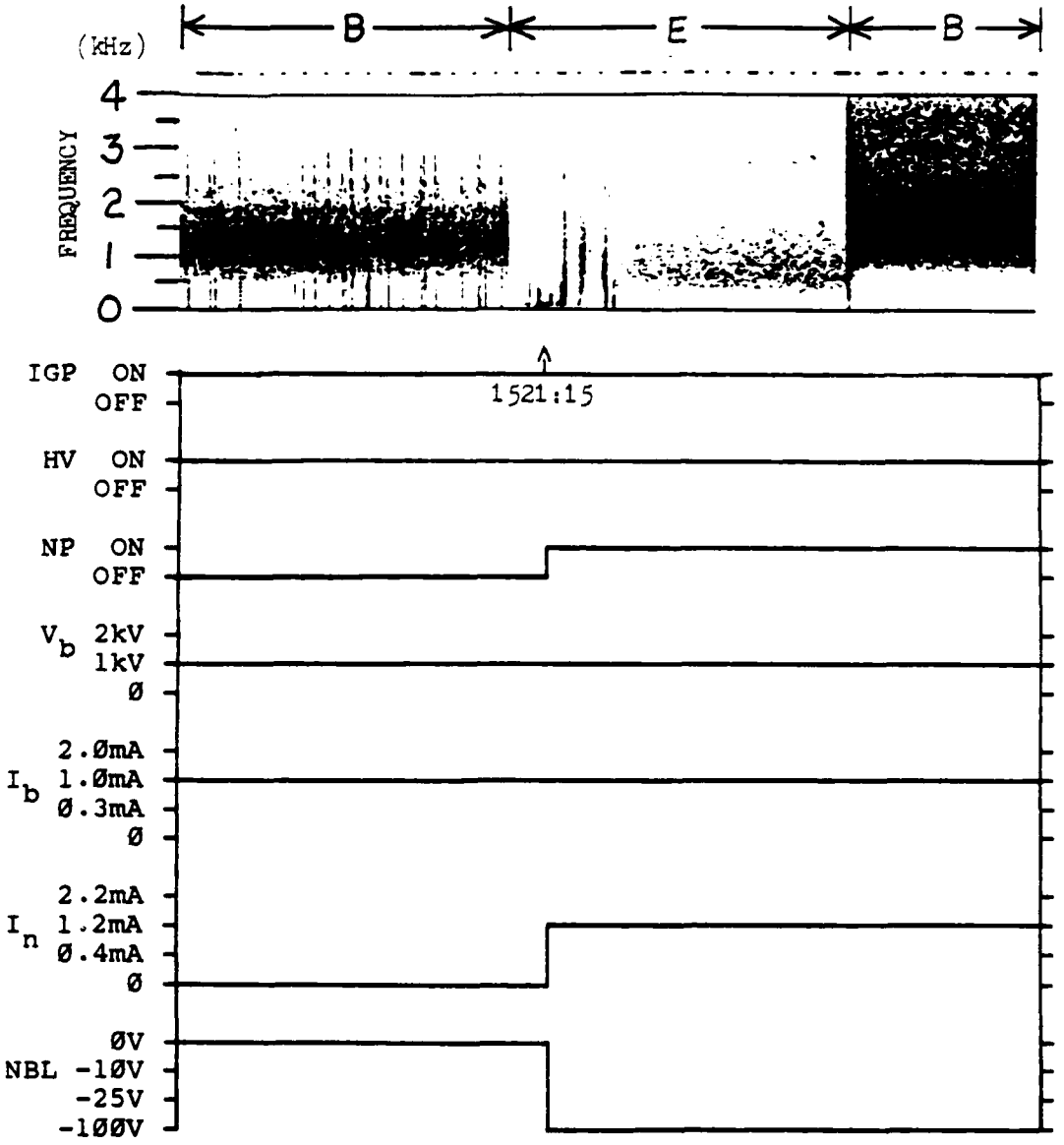

Figure 22. Spectrogram of the period 1520:58 - 1521:38 2 April 1979.

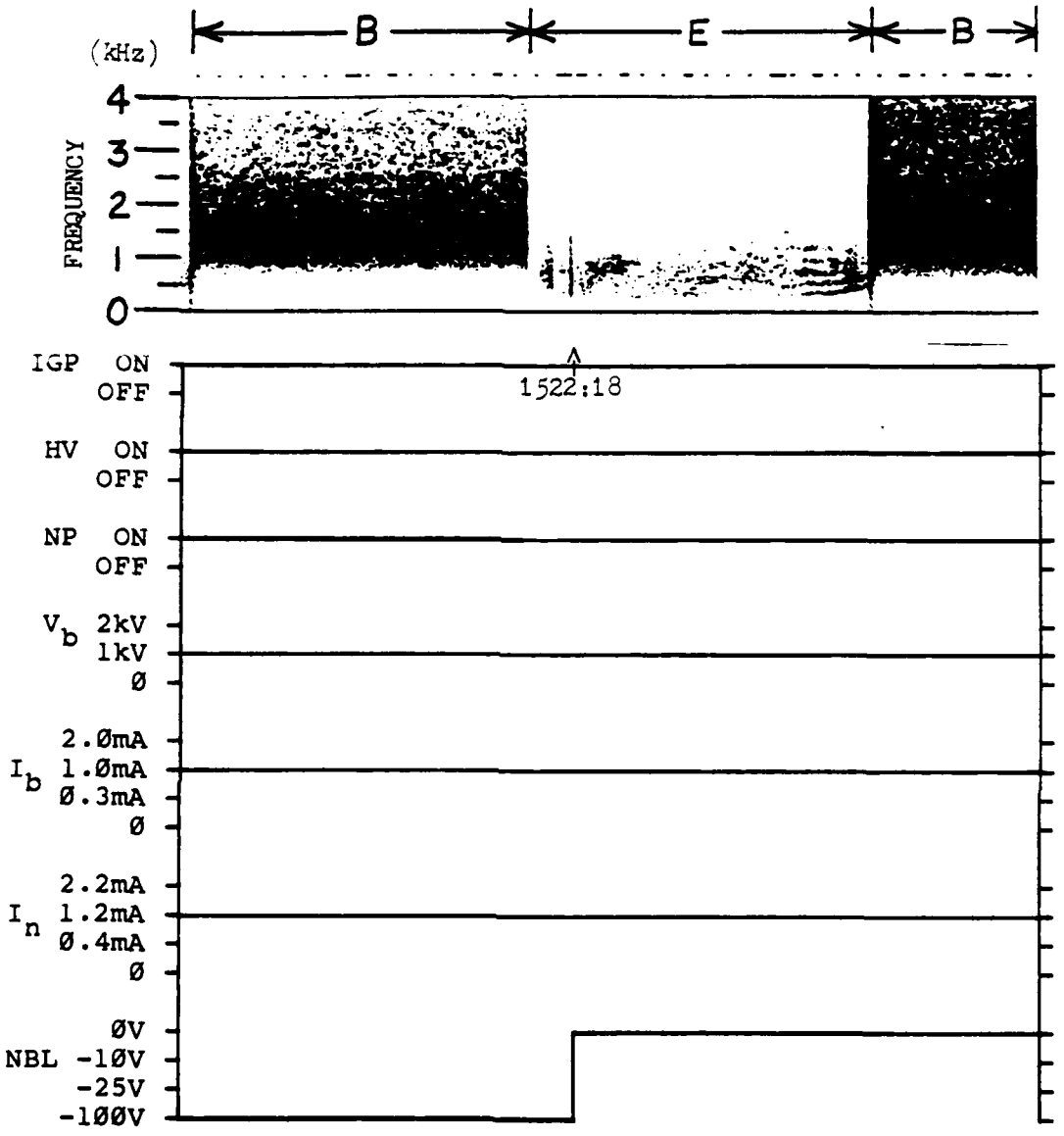

Figure 23. Spectrogram of the period 1522:00 - 1522:40 2 April 1979.

The lowest frequency signal is about 300 Hz and the frequency spacing between signals is about 170 Hz. Similar results were seen at other times when the bias level was 0 V. Bias level changes between different negative voltages had no effect on the electric field data.

At 1540:30 the satellite is no longer in eclipse and the ion gun power is turned off. Plasma wave data for this time is shown in Figure 24. The 700, 1400 and 2100 Hz interference lines are again visible in the magnetic field data. No signals are visible in the electric field data after the gun is turned off.

This operation is summarized in Figure 25. The narrowband filter data is shown for the period 1400 - 1600 UT. During this time there were two trickle mode operations. The electric and magnetic field data responded to trickle mode as on day 200. Other mode changes are difficult to analyze because they were done over a short period compared to the time scale of Figure 25. The 10 kHz and higher frequency channels show large amounts of signal activity in these bands. The day 200 data (Figure 17) showed these bands to be much quieter. This signal activity correlates well with the period of time during which the satellite was in eclipse. Assuming that this 'noise' also exists in the frequency channels lower than 10 kHz, these lower channels would be difficult to analyze even with the time scale expanded.

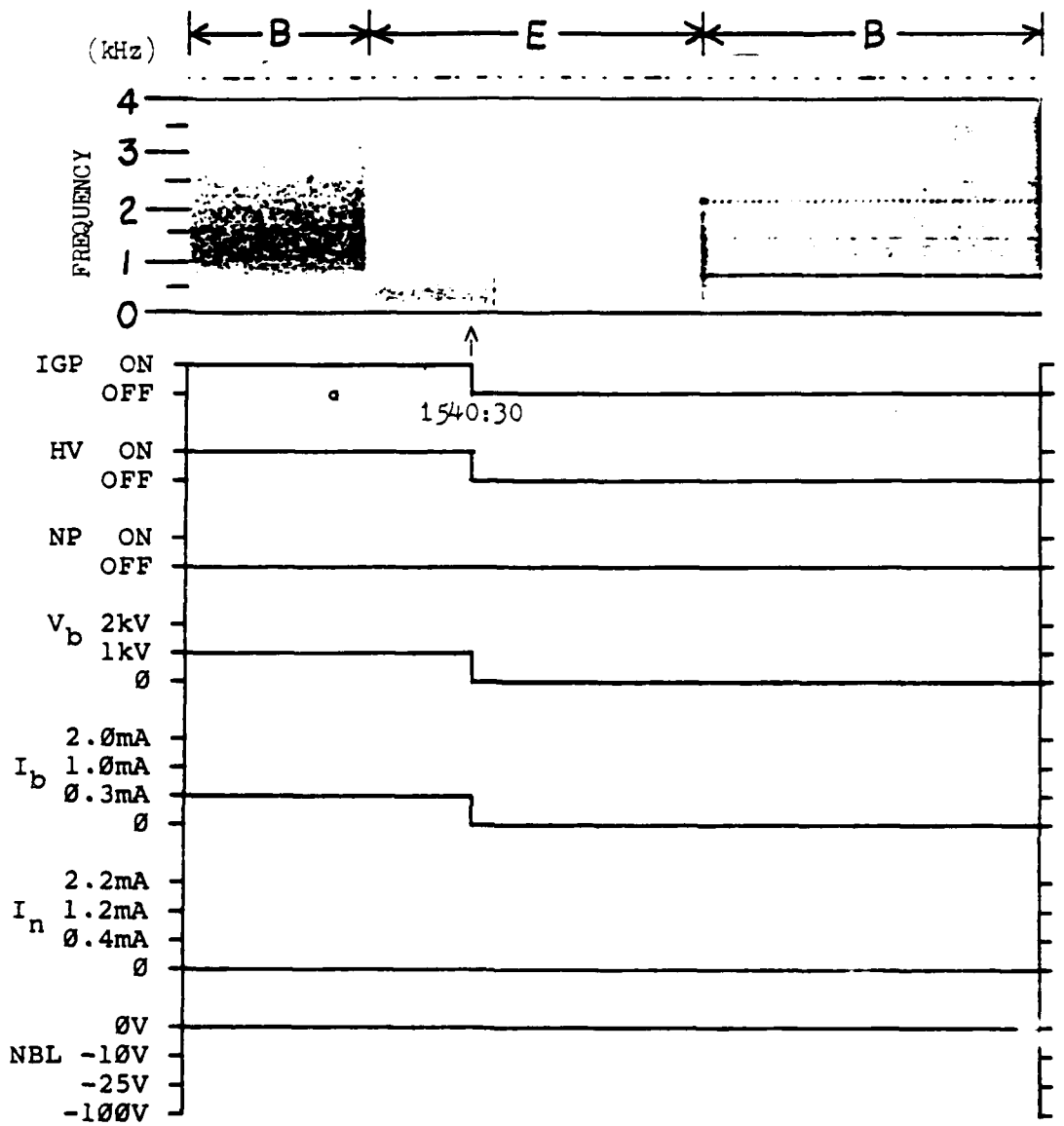

Figure 24. Spectrogram o he period 1540:14 - 1540:56 2 April 1979.

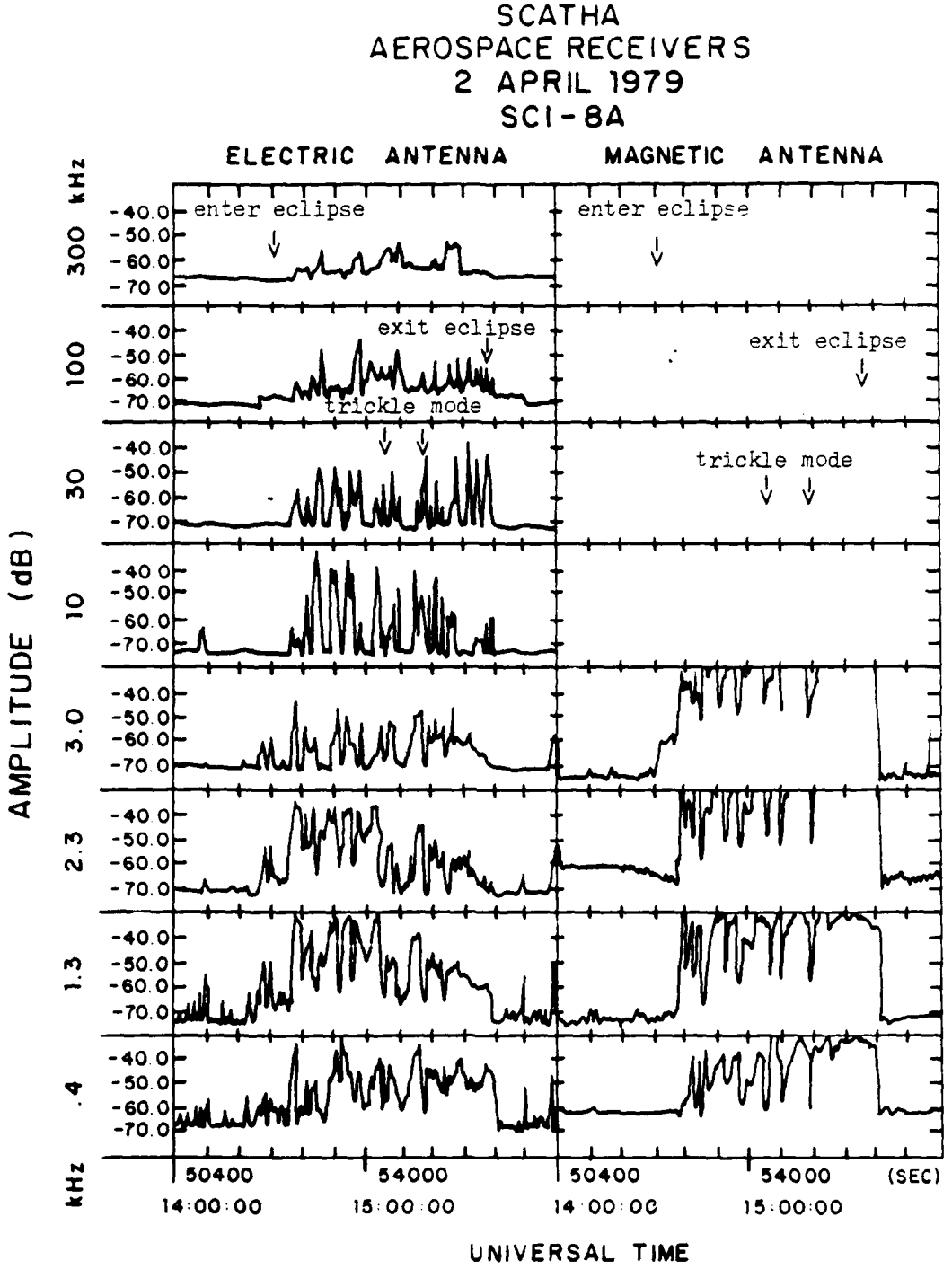

Figure 25. Narrowband filter data for 1400 - 1600 2 April 1979.

C. SUMMARY OF OBSERVATIONS

Broadband and narrowband plasma wave data taken during ion gun operations conducted on several different days were surveyed. Data presented above were chosen to show typical responses observed during neutral and non-neutral accelerated beam emissions and during trickle mode. Plasma wave response to ion gun operations did not show any dependence on satellite location within the magnetosphere.

Emission of a neutralized ion beam produced near zero satellite potentials (slightly positive due to higher electron current than ion current). The plasma wave data at such times show broadband signals recognized as the receiver response to a white noise input and occasional naturally occurring signals.

Non-neutralized beam operations were conducted to study the effects of negative charging on the satellite. Plasma wave data during these emissions show that for beam currents of 1 mA and higher, differential charging induced arcing is occurring.

Operation of the ion gun in trickle mode causes a cold, dense Xe^+ cloud to form in the vicinity of the satellite. No arcing occurs during this operating mode. The broadband data shows that white noise is being received by the magnetic field antenna and only natural signals appear in the electric field data. Examination of narrowband filter

data for this mode shows that input to the electric field antenna at 30 kHz and below is at gun-off background levels, while the magnetic field antenna is still receiving signals with amplitudes 20 - 30 dB above background. Hence, whatever signals are generated near the satellite do not interfere with plasma wave observations with the long electric field antenna. In addition, there should be shielding of the electric antenna from satellite generated signals due to attenuation in the Xe^+ cloud as shown next.

IV. CALCULATIONS

Propagation of electromagnetic waves through a plasma is a complex situation to analyze. In general, many simplifing assumptions are needed to allow solutions to be obtained. In order to estimate the attenuation of low frequency waves near the satellite we shall assume the following:

- wave frequency much exceeds the xenon ion cyclotron frequency ($f >> f_{ci}$).
- no pressure gradient effects (cold plasma).
- no external magnetic field ($B_o = \emptyset$).
- zero intrinsic impedance (collisionless plasma).

The density during trickle mode of the xenon plasma cloud around the satellite is not known but can be estimated. Typical hollow cathode density profiles as measured in a laboratory are shown in Figure 26 (Ref. 24). This experimental data shows a typical density a few centimeters from the cathode is between $1\emptyset^7$ cm^{-3} and $1\emptyset^8$ cm^{-3}. The density is seen to fall-off sharply with the density expected at 1 m to be about $1\emptyset^5$ cm^{-3} to $1\emptyset^6$ cm^{-3}. These density profiles should be comparable to those for the ion gun operated at geosynchronous orbit.

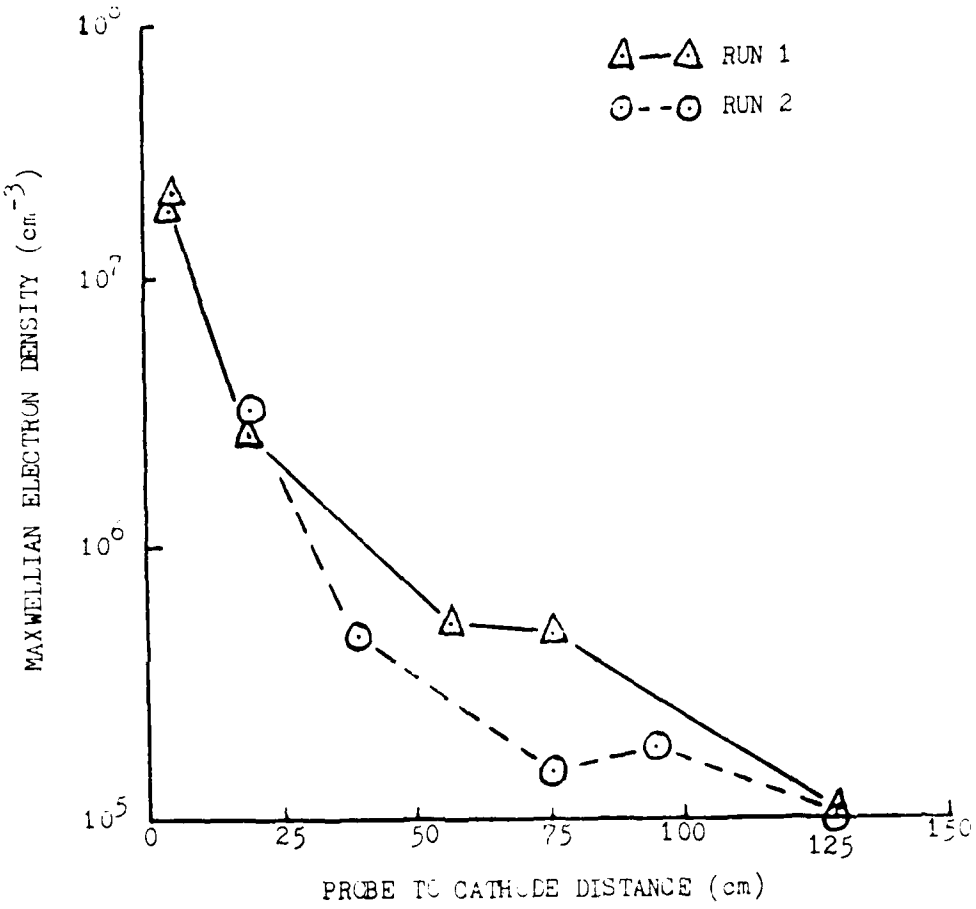

Figure 26. "Typical" hollow cathode density profiles in laboratory.

The dispersion relation for electromagnetic waves using the assumptions made above is

$$v^2 = \frac{c^2}{1 - \omega_p^2/\omega^2}$$

where v is the phase velocity in the plasma, ω is the wave frequency, ω_p is the plasma frequency, and c is the speed of light in a vacuum (Refs. 25,26). For our situation the plasma frequency is on the order of 10 kHz to 100 kHz and the wave frequencies we are concerned with are less than 10 kHz. When the wave frequency is less than the plasma frequency the phase velocity is imaginary and the wave is attenuated in the medium. If d is defined as the distance over which the wave amplitude decreases by a factor of 1/e, then

$$d = \frac{c}{\omega_p} \frac{1}{(1 - \omega^2/\omega_p^2)^{1/2}} \qquad \text{(Ref. 26).}$$

Using this expression one obtains the following attenuation distances (for 700 Hz).

$n\ (cm^{-3})$	d (m)
10^4	53
10^5	17
10^6	5.3
10^7	1.7
10^8	0.5

Densities of 10^4 cm^{-3} to 10^8 cm^{-3} would be consistent with available laboratory data, observations of signals near 100 kHz in the electric field data (xenon plasma frequency is 100 kHz for $n_{Xe} = 3 \times 10^7$ $1/cm^3$), and the attenuation of the interference lines.

The actual xenon density profile around the satellite is not known, and thus it is not possible to verify that attenuation is actually taking place. The disappearance of the tuning-fork interference lines from the magnetic field data during trickle mode could simply be an artifact caused by the AGC. However, it is consistent with theory and observation that low frequency wave attenuation by the dense xenon cloud generated during trickle mode is improving the data.

V. CONCLUSIONS

The positive emission system experiment on board the SCATHA satellite showed that a neutralized ion beam is very effective in discharging a differentially charged satellite. However, the plasma wave experiments on board SCATHA show that arcing can result from the operation of a non-neutralized ion beam. Some major points of interest in the data are:

- The arcing seen during emission of accelerated ions without neutralization depends on the beam current, with more frequent arcing at higher beam current.
- Arcing ceases when the acceleration voltage is turned off, while the gun is still emitting ions.
- Arcing ceases when the neutralizer is turned on.
- A broadband (1 - 2 kHz) signal exists on the magnetic antenna during trickle mode but not on the electric antenna.
- Intense low (<100 Hz) frequency signals seen in the electric field data with the gun off and during non-neutralized beam emissions are not seen during neutralized beam emissions.

If the arcing, is due to differential charging it is clear that it would be a function of the beam current level. Both trickle mode and neutralizer operations would provide a means of discharging the satellite causing the surface arcing to cease. For these reasons we believe the arcing is caused by differential charging of the satellite surface.

The signals seen in the magnetic field data during trickle mode could be associated with plasma turbulence or ion acoustic waves in close proximity to the satellite. It is not clear if these signals are electrostatic or electromagnetic (Ref. 12).

The broad (1 - 2 kHz) signal is regularly seen during ion gun operations. This signal is apparently the receiver response to a white noise input.

The emission of a neutralized ion beam, which is known to provide control of spacecraft charging, was found not to generate plasma waves which might interfere with the experimental observation of ambient signals. It is possible that the emission of a sufficiently dense, cold, neutral plasma (trickle mode with neutralizer on, bias level at Ø V) could allow the shielding of antennas (such as the SCIØ dipole antenna) from satellite interference while still allowing for control of satellite charging.

APPENDIX

TABLE 1

SCATHA SATELLITE EXPERIMENTS

Exp Id	Title	Parameters Measured
SC1	Engineering Experiments Plus VLF and HF Receivers	(1) Surface potentials of various materials (2) EM VLF wave analyzer (a few Hz to 300 kHz) (3) EM RF wave analyzer (2 MHz to 30 MHz) (4) Transient pulse shape analyzer
SC2	Spacecraft Sheath Fields Plus Energetic Ions	(1) Potentials of spherical probes (2) Low energy electrons and ions (15 eV/q to 18.6 keV/q) (3) Energetic protons (17 keV to >3.3 MeV) (4) Energetic ions $Z \geq 2$ (E_I >90 keV/neucleon)
SC3	High Energy Particle Spectrometer	High energy electrons and protons (E_e = 50 keV to 5.3 MeV, E_p = 1.0 MeV to 200 MeV)
SC4	Satellite Electron and Positive Ion Beam System	(1) Electron beam emission system E_e = 50 eV to 3.0 keV; I_e = 1.0 μA to 13 mA) (2) Positive ion (Xenon) beam emission system (E_I = 1.0 and 2.0 keV; I_I = 0.3 mA to 2.0 mA)
SC5	Rapid Scan Particle Detector	Electrons and ions (E_e = 50 eV to 1.0 MeV; E_I=50 eV to 35 MeV)

TABLE 1 - Continued.

Exp Id	Title	Parameters Measured
SC6	Thermal Plasma Analyzer	Thermal electrons and ions (E_e & E_I from Ø eV to 1ØØ eV)
SC7	Light Ion Mass Spectrometer	Light ion density, temperature and composition (E_I = Ø.Ø to 1ØØ eV; H^+, He^+, O^+)
SC8	Energetic Ion Composition Experiment	(1) Ion composition of energetic plasma (E_I = 1ØØ eV to 32 keV; M^I= Ø.8 to 16Ø AMU with M/Q= 1,2,4 or 16) (2) Low energy electrons (E_e = 7Ø eV to 24 keV in 4 channels)
SC9	UCSD Charged Particle Experiment	Electrons and ions (one set with E = few eV to 81 keV, two others with E = Ø.2 eV to 1.55 keV)
SC1Ø	Electric Field Detector	DC and ELF electric fields and satellite potential (ELF Ø.2 to 2ØØ Hz; common mode voltage Ø to ± 5 keV)
SC11	Magnetic Field Monitor	DC and ELF magnetic field (range from ± Ø.3 to ± 5ØØ nT; ELF about 1 to 1ØØ Hz)
ML12	Spacecraft Contamination Plus Thermal Control Materials Monitoring	(1) Contaminant mass deposition rates (2) Solar absorptance of test materials
TPM	Transient Pulse Monitor	Electromagnetic pulse environment on satellite (Pulse amplitude 2 mV to 24Ø V, current 2 mA to 17ØØ A)

TABLE 2

SC4-2 ION GUN COMMANDS

Command	Function
1. Instrument on	Turns on instrument power
2. Instrument off	Turns off all instrument power
3. Expellant valve open	Opens solenoid valve
4. Expellant valve closed	Closes expellant valve
5. Cathode heater preheat	Turns on the cathode to Level 1 and turns on discharge supply
6. Ion gun power on	Turns on the ion gun power
7. Ion gun power off	Turns off the ion gun power
8. Beam voltage Level 1	Sets the beam power supply to 1000 V
9. Beam voltage Level 2	Sets the beam power supply to 2000 V
10. Keeper off	Turns the keeper supply off
11. Discharge current and neutralizer emission Level 1	Sets the discharge current reference to achieve 20 mA current; sets neutralizer emission level to 0.4 mA
12. Discharge current and neutralizer emission Level 2	Sets the discharge current reference to achieve 125 mA current; sets neutralizer emission level to 1.2 mA
13. Discharge current and neutralizer emission Level 3	Sets the discharge current reference to achieve 200 mA current; sets neutralizer emission level to 2.2 mA
14. Neutralizer emission Level 4	Sets neutralizer emission level to 2 μA

TABLE 2 - Continued.

Command	Function
15. Neutralizer emission Level 5	Sets neutralizer emission level to 20 μA
16. Neutralizer No. 1	Selects neutralizer filament No. 1
17. Neutralizer No. 2	Selects neutralizer filament No 2
18. Neutralizer heater on	Turns on the neutralizer cathode heater
19. Neutralizer heater off	Turns off the neutralizer heater
20. Neutralizer bias off	Turns off the neutralizer bias power supply
21. Neutralizer bias positive	Sets the neutralizer bias for positive polarity
22. Neutralizer bias negative	Sets the neutralizer bias for negative polarity
23. Neutralizer bias Level 1	Turns on the neutralizer bias to 10 V
24. Neutralizer bias Level 2	Turns on the neutralizer bias to 25 V
25. Neutralizer bias Level 3	Turns on the neutralizer bias to 100 V
26. Neutralizer bias Level 4	Turns on the neutralizer bias to 500 V
27. Neutralizer bias Level 5	Turns on the neutralizer bias to 1000 V
28. High voltage off	Turns off the beam and accel power supplies
29. Cathode conditioning	Turns on the cathode heater

LIST OF REFERENCES

1. Olsen, R. C., "Observations of Charging Dynamics," Journal of Geophysical Research, v. 88, p. 5657, 1 July 1983.

2. Grard, R., Knott, K. and Pedersen, "Spacecraft Charging Effects," Space Science Reviews, v. 34, pp. 289-304, 1983.

3. Garrett, H. B., "The Charging of Spacecraft Surfaces," Reviews of Geophysics and Space Physics, v. 19, pp. 577-616, November 1981.

4. Whipple, E. C., Potentials of Surfaces in Space, pp. 1-65, University of California at San Diego, La Jolla, California, February 1981.

5. Kintner, P. M. and Kelley, M. C., "Plasma Waves Produced by the Xenon Ion Beam Experiment on the Porcupine Sounding Rocket," in Artificial Partical Beams in Space Plasma Studies, pp. 199-205, edited by Grandal, B., NATO Advanced Study Institute Series, Series B, v. 79, 1982.

6. Kintner, P. M. and Kelley, M. C., "Ion Beam Produced Plasma Waves Observed by the Delta n/n Plasma Wave Receiver During the Porcupine Experiment," in Advances in Space Research, Active Experiments in Space Plasmas, v. 1, n. 2, pp. 107-115, edited by Russell, C. T. and Rycroft, M. J., Pergamon Press Ltd., Oxford OX3 0BW, England, 1981.

7. Kintner, P. M. and Kelley, M. C., "A Perpendicular Ion Beam Instability: Solutions to the Linear Dispersion Relation," Journal of Geophysical Research, v. 88, pp. 357-359, 1 January 1983.

8. Jones, D., "Xe^{+}-Induced Ion-Cyclotron Harmonic Waves," in Advances in Space Research, Active Experiments in Space Plasmas, v. 1, n. 2, pp. 103-106, edited by Russell, C. T. and Rycroft, M. J., Pergamon Press Ltd., Oxford OX3 0BW, England, 1981.

9. Walker, D. N., "Perpendicular Ion Beam-Driven Instability in a Multicomponent Plasma: Effects of Varying Ion Composition on Linear Flute Mode Oscillations," Journal of Geophysical Research, v. 91, p. 3305, 1 March 1986.

10. Hudson, M. K. and Roth, I., "Thermal Fluctuations From an Artificial Ion Beam Injection Into the Ionosphere," Journal of Geophysical Research, v. 89, pp. 9812-9813, 1 November 1984.

11. Erlandson, R. E., and others, "Initial Results From the Operation of Two Argon Ion Generators in the Auroral Ionosphere," Journal of Geophysical Research, v. 92, pp. 4601-4608, 1 May 1987.

12. Haerendel, G. and Sagdeev, R. Z., "Artificial Plasma Jet in the Ionosphere," in Advances in Space Research, Active Experiments in Space Plasmas, v. 1, n. 2, pp. 29-46, edited by Russell, C. T. and Rycroft, M. J., Pergamon Press Ltd., Oxford OX3 0BW, England, 1981.

13. Roth, I., and others, "Simulations of Beam Excited Minor Species Gyroharmonics in the Porcupine Experiment," Journal of Geophysical Research, v. 88, pp. 8115-8122, 1 October 1983.

14. Fennell, J. F., "Description of P78-2 (SCATHA) Satellite and Experiments," in IMS Source Book, pp. 65-78, AGU, Washington D.C., 1982.

15. Olsen, R. C., Electron Beam Experiments at High Altitudes, paper presented at NATO meeting, June 1986.

16. Air Command and Staff College, Air University, Maxwell Air Force Base, Space Handbook, p. 1-13, Government Printing Office, Washington, D.C., 1985.

17. Masek, T. D. and Cohen, T. D., "Satellite Positive-Ion-Beam System," Journal of Spacecraft and Rockets, v. 15, pp. 27-33, 1 January/February 1978.

18. Koons, H. C. and Cohen, H. A., "Plasma Waves and Electrical Discharges Stimulated by Beam Operations on a High Altitude Satellite," in Artificial Particle Beams in Space Plasma Studies, pp. 111-120, edited by Grandal, B., NATO Advanced Study Institute Series, Series B, v. 79, 1982.

19. Koons, H. C., and others, "Observations of Electron Cyclotron Harmonic Emissions Associated With Field - Aligned Electron Beams," Journal of Geophysical Research, v. 92, pp. 7531-7537, 1 July 1987.

20. Olsen, R. C., private communication, 1987.

21. Chen, F. F., Introduction to Plasma Physics and Controlled Fusion, 2nd ed., v. 1, pp. 95-98, 267-273, Plenum Press, 1984.

22. Kadomtsev, B. B.. Plasma Turbulence. Translated by Ronson, L. C.. Edited by Rusbridge, M. G.. pp. 35-39. Academic Press, New York, 1965.

23. Olsen, R. C., "Modification of Spacecraft Potentials by Plasma Emission," Journal of Spacecraft and Rockets, v. 18, pp. 462-469, September/October 1981.

24. Wilbur, P. and Williams, J., Unpublished work using hollow cathodes in laboratory tests, Colorado State University, 1986.

25. Chen, F. F., Introduction to Plasma Physics and Controlled Fusion, 2nd ed., v. 1, pp. 79-131, Plenum Press, 1984.

26. Spitzer, L. Jr., Physics of Fully Ionized Gases, pp. 47-55, Interscience Publishers, Inc., 1956.

BIBLIOGRAPHY

Craven, P. D., and others, "Potential Modulation on the SCATHA Spacecraft," Journal of Spacecraft and Rockets, v. 24, March/April 1987.

DeForest, S. E., "Spacecraft Charging at Synchronous Orbit," Journal of Geophysical Research, v. 77, 1 February 1972.

Fennell, J. F., and others, "A Review of SCATHA Results: Charging and Discharging," Proceedings of the ESLAB Symposium on 'Spacecraft/Plasma Interactions and their Influence on Field and Particle Measurements', Noordwijk, The Netherlands, 13-16 September 1983. (ESA SP-198, publ. December 1983).

Kelley, M. C. and Pfaff, R. F., "Electric Field Measurements During the Condor Critical Velocity Experiment," Journal of Geophysical Research, v. 91, 1 September 1986.

Koons, H. C., "The Role of Hiss in Magnetospheric Chorus Emissions," Journal of Geophysical Research, v. 86, 1 August 1981.

Koons, H. C. and Fennell, J. F., "Particle and Wave Dynamics During Plasma Injections," Journal of Geophysical Research, v. 88, 1 August 1983.

Koons, H. C., "Whistlers and Whistler-Stimulated Emissions in the Outer Magnetosphere," Journal of Geophysical Research, v. 90, 1 September 1985.

Koons, H. C. and Edgar, B. C., "Observations of VLF Emissions at the Electron Gyrofrequency," Journal of Geophysical Research, v. 90, 1 November 1985.

Lai, S. T., and others, "Boom Potential of a Rotating Satellite in Sunlight," Journal of Geophysical Research, v. 91, 1 November 1986.

Mizera, P. F., and others, "First Results of Material Charging in the Space Environment," Applied Physics Letters, v. 37, 1 August 1980.

Mullen, E. G., and others, "SCATHA Survey of High-Level Spacecraft Charging in Sunlight," Journal of Geophysical Research, v. 91, 1 February 1986.

Olsen, R. C., "Differential and Active Charging Results from the ATS Spacecraft." Ph.D. dissertation, University of California, San Diego, July 1980.

Olsen, R. C., "The Hidden Ion Population of the Magnetosphere," Journal of Geophysical Research, v. 87, 1 May 1982.

Olsen, R. C., "A Threshold Effect for Spacecraft Charging," Journal of Geophysical Research, v. 88, 1 January 1983.

Olsen, R. C., "Experiments in Charge Control at Geosynchronous Orbit - ATS-5 and ATS-6," Journal of Spacecraft and Rockets, v. 22, May/June 1985.

Olsen, R. C., "Observations of Electric Fields Near the Plasmapause at Midnight," Journal of Geophysical Research, v. 91, 1 November 1986.

Olsen, R. C., and others, "Plasma Observations at the Earth's Magnetic Equator," Journal of Geophysical Research, v. 92, 1 March 1987.

Yau, A. W., and others, "Particle and Wave Observations of Low-Altitude Ionospheric Ion Acceleration Events," Journal of Geophysical Research, v. 88, 1 January 1983.

INITIAL DISTRIBUTION LIST

		No. Copies
1.	Defense Technical Information Center Cameron Station Alexandria, Virginia 22304-6145	2
2.	Library, Code 0142 Naval Postgraduate School Monterey, California 93943-5002	2
3.	Department Chairman, Code 61 Department of Physics Naval Postgraduate School Monterey, California 93943	2
4.	Dr. R. C. Olsen, Code 61OS Department of Physics Naval Postgraduate School Monterey, California 93943	20
5.	Dr. S. Gnanalingam, Code 61GM Department of Physics Naval Postgraduate School Monterey, California 93943	1
6.	Ms. D. E. Donatelli Space Physics Division Air Force Geophysics Laboratory/PH Hanscom AFB, Massachusetts 01731	1
7.	Dr. R. Sagalyn Space Physics Division Air Force Geophysics Laboratory/PH Hanscom AFB, Massachusetts 01731	1
8.	Mr. G. Mullen Space Physics Division Air Force Geophysics Laboratory/PHP Hanscom AFB, Massachusetts 01731	1
9.	Dr. S. Lai Space Physics Division Air Force Geophysics Laboratory/PH Hanscom AFB, Massachusetts 01731	1

10. Dr. B. Burke — 1
Space Physics Division
Air Force Geophysics Laboratory/PHA
Hanscom AFB, Massachusetts 01731

11. Dr. N. Maynard — 1
Space Physics Division
Air Force Geophysics Laboratory/PH
Hanscom AFB, Massachusetts 01731

12. Mr. H. A. Cohen — 1
W. J. Schafer Associates
1901 North Fort Meyer Drive
Arlington, Virginia 22209

13. Mr. R. Gracen Joiner — 1
Office of Naval Research, Code 1114
800 North Quincy Street
Arlinton, Virginia 22217-5000

14. Dr. H. C. Koons — 3
Space Sciences Laboratory
The Aerospace Corporation, M2/260
P. O. Box 92957
Los Angeles, California 90009

15. Dr. J. Roeder — 2
Space Sciences Laboratory
The Aerospace Corporation, M2/260
P. O. Box 92957
Los Angeles, California 90009

16. Dr. E. C. Whipple — 1
Center for Astrophysics and Space Science
University of California at San Diego
La Jolla, California 92093

17. Dr. C. E. McIlwain — 1
Center for Astrophysics and Space Science
University of California at San Diego
La Jolla, California 92093

18. Dr. J. Hyman — 1
Hughes Research Lab
3011 Malibu Canyon Road
Malibu, California 90265

19. Dr. T. Williamson — 1
Hughes Research Lab
3011 Malibu Canyon Road
Malibu, California 90265

20. Dr. S. Shawhan — 1
NASA Headquarters/E
Washington, DC 20546

21. Dr. C. K. Purvis — 1
MC 302-1
NASA Lewis Research Center
21000 Brookpark Road
Cleveland, Ohio 44135

22. Dr. J. Kolecki — 1
MC 302-1
NASA Lewis Research Center
21000 Brookpark Road
Cleveland, Ohio 44135

23. Dr. C. R. Chappell — 1
NASA Marshall Space Flight Center
Huntsville, Alabama 35812

24. Dr. T. E. Moore, ES53 — 1
NASA Marshall Space Flight Center
Huntsville, Alabama 35812

25. Dr. J. H. Waite, ES53
NASA Marshall Space Flight Center
Huntsville, Alabama 35812

26. Dr. D. Hastings — 1
Department of Aeronautics and Astronautics
Massachusetts Institute of Technology
Cambridge, Massachusetts 02139

27. Dr. I. Katz — 2
S - Cubed
P. O. Box 1620
La Jolla, California 92038-1620

28. Dr. J. Raitt — 1
CASS
Utah State University
Logan, Utah 84322

29. Professor Nobuki Kawashima 1
Institute of Space and Astronautical Science
Komaba 4 - chome
Meguro - ku
Tokyo, Japan 153

30. Professor W. Riedler 1
Institute fuer Weltraumforschung Oesterreichische
Akademieder Wissenschaften
Inffeldgasse 12
A - 8810 Graz, Austria

31. Dr. K. Torkar 1
Institute fuer Weltraumforschung Oesterreichische
Akademieder Wissenschaften
Inffeldgasse 12
A - 8810 Graz, Austria

32. Dr. R. Schmidt 1
Space Science Department
ESA/ESTEC
Noordwijk, The Netherlands

33. Dr. A. Pedersen 2
Space Science Department
ESA/ESTEC
Noordwijk, The Netherlands

34. LT L. E. Weddle, USN 1
10085 West Georgetown Road
Columbus, Indiana 47201

35. Dr. W. F. Denig 1
Space Physics Division
Air Force Geophysics Laboratory/PHG
Hanscom AFB, Massachusetts 01731

36. Dr. N. Omidi 1
IGPP
University of California at Los Angeles
Los Angeles, California 90024

37. Dr. Maha Ashour - Abdalla 1
IGPP
University of California at Los Angeles
Los Angeles, California 90024

38. Dr. R. R. Anderson 1
Department of Physics and Astronomy
University of Iowa
Iowa City, Iowa 52242

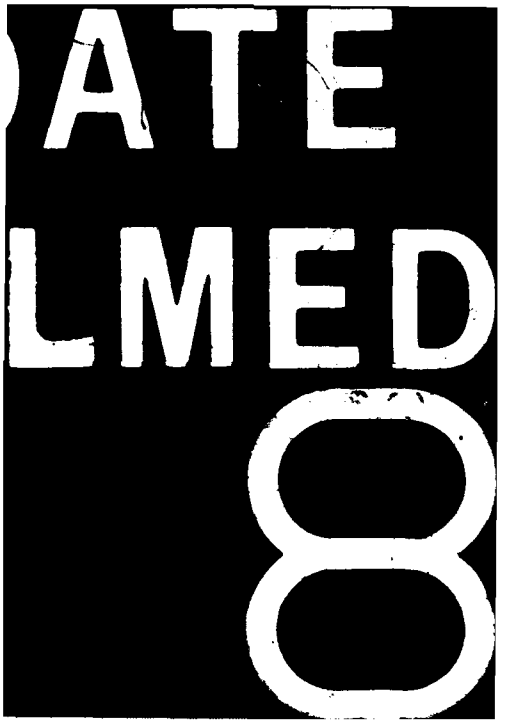
ATE
LMED
8